Published in final edited form as:
Neuroscience. 2006 June 30; 140(2): 433–451.

ASSOCIATION OF CONNEXIN36 AND ZONULA OCCLUDENS-1 WITH ZONULA OCCLUDENS-2 AND THE TRANSCRIPTION FACTOR ZONULA OCCLUDENS-1-ASSOCIATED NUCLEIC ACID-BINDING PROTEIN AT NEURONAL GAP JUNCTIONS IN RODENT RETINA

C. CIOLOFAN[a,1], **X.-B. LI**[a,1], **C. OLSON**[a], **N. KAMASAWA**[b], **B. R. GEBHARDT**[b], **T. YASUMURA**[b], **M. MORITA**[b], **J. E. RASH**[b], and **J. I. NAGY**[a,*]

a*Department of Physiology, Faculty of Medicine, University of Manitoba, 730 William Avenue, Winnipeg, Manitoba, Canada R3E 3J7*

b*Department of Biomedical Sciences, Colorado State University, Fort Collins, CO 80523, USA*

Abstract

Most gap junctions between neurons in mammalian retina contain abundant connexin36, often in association with the scaffolding protein zonula occludens-1. We now investigate co-association of connexin36, zonula occludens-1, zonula occludens-2 and Y-box transcription factor 3 (zonula occludens-1-associated nucleic acid-binding protein) in mouse and rat retina. By immunoblotting, zonula occludens-1-associated nucleic acid-binding protein and zonula occlu-dens-2 were both detected in retina, and zonula occludens-2 in retina was found to co-immunoprecipitate with connexin36. By immunofluorescence, the four proteins appeared as puncta distributed in the plexiform layers. In the inner plexiform layer, most connexin36-puncta were co-localized with zonula occludens-1, and many were co-localized with zonula occludens-1-associated nucleic acid-binding protein. Moreover, zonula occludens-1-associated nucleic acid-binding protein was often co-localized with zonula occludens-1. Nearly all zonula occludens-2-puncta were positive for connexin36, zonula occludens-1 and zonula occludens-1-associated nucleic acid-binding protein. In the outer plexiform layer, connexin36 was also often co-localized with zonula occludens-1-associated nucleic acid-binding protein. In connexin36 knockout mice, labeling of zonula occludens-1 was slightly reduced in the inner plexiform layer, zonula occludens-1-associated nucleic acid-binding protein was decreased in the outer plexiform layer, and both zonula occludens-1-associated nucleic acid-binding protein and zonula occludens-2 were markedly decreased in the inner sublamina of the inner plexiform layer, whereas zonula occludens-1, zonula occludens-2 and zonula occludens-1-associated nucleic acid-binding protein puncta persisted and remained co-localized in the outer sublamina of the inner plexiform layer. By freeze-fracture replica immunogold labeling, connexin36 was found to be co-localized with zonula occludens-2 within individual neuronal gap junctions. In addition, zonula occludens-1-associated nucleic acid-binding protein was abundant in a portion of ultrastructurally-defined gap junctions throughout the inner plexiform layer, and some of these junctions contained both connexin36 and zonula occludens-1-associated nucleic acid-binding protein. These distinct patterns of connexin36 association with zonula occludens-1, zonula occludens-2 and zonula occludens-1-associated nucleic acid-binding protein in different sublaminae of retina, and differential responses of these proteins to connexin36 gene deletion suggest differential regulatory and scaffolding roles of these gap junction accessory proteins. Further, the persistence of

[1]Contributed equally as first authors to the present work.

[*]Corresponding author. Tel: +1-204-789-3767; fax: +1-204-789-3934. E-mail address: nagyji@ms.umanitoba.ca (J. I. Nagy).

a subpopulation of zonula occludens-1/zonula occludens-2/zonula occludens-1-associated nucleic acid-binding protein co-localized puncta in the outer part of the inner plexiform layer of connexin36 knockout mice suggests close association of these proteins with other structures in retina, possibly including gap junctions composed of an as-yet-unidentified connexin.

Keywords

neurons; electrical synapses; gap junctions; PDZ domains; scaffolding proteins

Neuronal gap junctions are the structural correlates of electrical synapses, allowing electrical coupling as well as passage of ions and small molecules between cells (Bennett, 1997). The intercellular channels at these junctions are composed of various members of the 21 identified gap junction-forming connexin (Cx) family of proteins (Goodenough et al., 1996; Kumar and Gilula, 1996; Willecke et al., 2002). Among the diverse structures in which electrical synapses have now been identified in mammalian CNS (Bennett and Zukin, 2004; Connors and Long, 2004), the retina is considered an ideal model system in which to study the contribution of such synapses to processing of signals in neural pathways (Vaney, 1999). Retina contains a high density of gap junctions that produce complex patterns of circuitry interlinking specific classes of neurons (Becker et al., 1998; Sharpe and Stockman, 1999; Janssen-Bienhold et al., 2001). Connexins that form electrical synapses via gap junctions between various cell types in rodent retina include connexin36 (Cx36), Cx45 and Cx57 (Rash et al., 2000; Söhl et al., 2000; Güldenagel et al., 2000; Feigenspan et al., 2001, 2004; Hombach et al., 2004; Ciolofan et al., unpublished observations; Schubert et al., 2005), and expression of Cx50 mRNA was additionally reported in rabbit retina (Massey et al., 2003; Huang et al., 2005). The retina also is an ideal system for analyses of the regulation of electrical synapses by ambient illumination, neurotransmitters and intracellular signaling pathways (Vaney, 1999; Weiler et al., 1999, 2000; He et al., 2000). Such regulation not only involves local interaction with neurotransmitter receptors, but also interactions between gap junction-associated accessory proteins that may govern gap junctional conductance state and/or connexin trafficking via various signaling processes (Giepmans, 2004; Hervé et al., 2004). For example, the multi-functional PDZ (postsynaptic protein PSD95/*Drosophila* junction protein Disc-large/zonula occludens-1) domain-containing scaffolding protein zonula occludens-1 (ZO-1) has been found at gap junctions, where it interacts with the c-terminus of several different connexins (Giepmans and Moolenaar, 1998; Toyofuku et al., 1998; Kausalya et al., 2001; Laing et al., 2001; Nielsen et al., 2002, 2003; Li et al., 2004a,b,c; Penes et al., 2005). However, the regulatory and/or structural role of connexin/ZO-1 interaction remains obscure.

We have previously reported Cx36 co-localization with ZO-1 at neuronal gap junctions in mouse brain and retina, and direct interaction of the c-terminus of Cx36 with the first of the three PDZ-domains in ZO-1 (Li et al., 2004a; Rash et al., 2004). In a search for proteins that interact with ZO-1 at gap junctions and that, together with ZO-1, may serve regulatory roles at these junctions, we recently found association of ZO-1 with ZONAB (zonula occludens-1-associated nucleic acid binding protein; originally referred to as mouse Y-box transcription factor 3 [MsY3]) at gap junctions between glial cells in mouse brain (Penes et al., 2005). ZONAB was previously reported to interact with ZO-1 at tight junctions of cultured MDCK cells, where it may have a role in regulation of cell division, contact inhibition and tumorigenesis (Balda and Matter, 2000, 2003; Balda et al., 2003). In addition, zonula occludens-2 (ZO-2) expression has been reported in retina (Collins and Rizzolo, 1998), and this protein is a well-established interaction partner of ZO-1 at tight junctions in various tissues (González-Mariscal et al., 2000, 2003). In the present study, we provide immunofluorescence and freeze-fracture replica immunogold labeling (FRIL) evidence for neuronal expression of ZONAB and ZO-2 in mouse and rat retina, and demonstrate differential spatial associations

and ultrastructural localizations of Cx36, ZO-1, ZO-2 and ZONAB in retina of wild-type (WT) and Cx36 knockout (KO) mice.

EXPERIMENTAL PROCEDURES

Antibodies and animals

Antibodies used in this study, together with sequence specificity, dilutions employed and source, are presented in Table 1. Affinity-purified rabbit polyclonal and mouse monoclonal anti-connexin and anti-ZO-1 antibodies were obtained from Invitrogen/Zymed Laboratories (South San Francisco, CA, USA). A recently available polyclonal antibody generated against a peptide corresponding to sequence within mouse ZONAB was also obtained from Invitrogen/Zymed Laboratories. Specificities of the anti-Cx36 and anti-ZO-1 antibodies used were demonstrated elsewhere (Li et al., 2004a,b;Penes et al., 2005). Mouse anti-ZO-2 antibody was obtained from BD Biosciences (Mississauga, ON, Canada) and rabbit anti-ZO-2 from Invitrogen/Zymed Laboratories. Goat polyclonal anti-calretinin Ab1550 was purchased from Chemicon International (Temecula, CA, USA). The anti-ZONAB antibody was developed against the mouse ortholog of canine ZONAB, referred to in GenBank as MsY3, or alternatively, as cold shock domain protein. The peptide epitope of anti-ZONAB is contained within a region of ZONAB that is present in both a long (ZONAB B) isoform of this protein, as well as its shorter, alternatively spliced isoform (ZONAB A), several versions of which are listed in the GenBank database (ZONAB A, accession No. AAF72335; ZONAB B, accession No. AAF72336; MsY-box 3 short form, accession No. AAG14419; MsY-box 3 long form, accession No. AAG14418; cold shock domain protein A short form, accession No. AAH62377; cold shock domain protein A long form, accession No. AAH48242). A total of 35 adult male CD1 mice, 10 male WT and five Cx36 KO C57BL6/129SvEv mice and two adult Sprague–Dawley rats obtained from animal facilities at our institutions were used in this study. All animals used in this study were prepared under protocols approved by the Institutional Animal Care and Use Committees of Colorado State University and the University of Manitoba. These protocols included minimization of stress to animals and number of animals used.

ZONAB expression vector and cell transfection

A bacterial cDNA clone containing the full-length coding region for mouse ZONAB (cold shock domain protein A; I.M.A.G.E. clone ID 6530404, GenBank accession number BC062377), corresponding to MsY3 short form and the mouse ortholog of canine ZONAB A, was obtained from American Type Culture Collection (ATCC) (Rockville, MD, USA) ATCC number 10470249. Selected colonies were incubated overnight at 37 °C in LB media supplemented with 50 μg/ml penicillin. Plasmid was extracted using the QIAprep Spin Miniprep Kit (Qiagen Inc., Mississauga, ON, Canada), cut with *Apa*I enzyme and separated by electrophoresis to confirm ZONAB coding region orientation. Plasmid DNA was digested using *Xba*I and *Eco*RV enzymes and the ZONAB coding region was ligated into pcDNA3.1 expression vector (Invitrogen Life Technologies, Burlington, ON, Canada) using T4 DNA ligase. DH5α *E. coli* cells (Invitrogen Life Technologies) were transformed with ZONAB-pcDNA3.1 recombinant plasmid according to manufacturer's instructions, then plated on ampicillin containing agar plates and incubated overnight at 37 °C. Transformed colonies were selected and amplified overnight at 37 °C in LB media supplemented with 50 μg/ml penicillin. The ZONAB-pcDNA3.1 recombinant plasmid was extracted, and an aliquot was digested with *Xba*I and *Eco*RV and separated by electrophoresis for recombinant product verification. HeLa cells (ATCC), grown in Dulbecco's Modified Eagle's Medium supplemented with 10% fetal bovine serum and 1% penicillin–streptomycin, were transiently transfected with pcDNA3.1 or ZONAB-pcDNA3.1 using LipofectAMINE 2000 reagent, as previously described (Li et al., 2004a,b). Transiently transfected HeLa cells were taken for analysis after a 24 h transfection period.

Western blotting

Mice were deeply anesthetized followed by decapitation and removal of the eyes. Retinas were dissected, rapidly frozen and stored at −80 °C until future use. ZONAB-transfected and empty vector-transfected control HeLa cells were rinsed with PBS buffer (50 mM sodium phosphate buffer, pH 7.4, 0.9% saline) and both HeLa cells and retinas were homogenized in immunoprecipitation (IP) buffer (20 mM Tris–HCl, pH 8.0, 140 mM NaCl, 1% Triton X-100, 10% glycerol, 1 mM EGTA, 1.5 mM $MgCl_2$, 1 mM dithiothreitol, 1 mM phenylmethylsulfonyl fluoride and 5 μg/ml each of leupeptin, pepstatin A and aprotinin) and sonicated. Retinal homogenates were taken for Western blotting immediately after homogenization. Freeze-thawing of homogenates appeared to result in protein degradation and detection of additional bands on immunoblots. Samples of retina were cleared of cellular debris by centrifugation at 20,000×*g* for 5 min and the supernatants were taken for protein determination using a kit (Bio-Rad Laboratories, Hercules, CA, USA). Western blotting was performed as previously described (Li et al., 2004a,b). A total of 50–100 μg of protein per lane was separated electrophoretically by sodium dodecylsulfate (SDS)–polyacrylamide gel electrophoresis (SDS-PAGE) using 10% or 12.5% gels, followed by transblotting to polyvinylidene difluoride membranes (Bio-Rad Laboratories) in standard Tris–glycine transfer buffer, pH 8.3, containing 0.5% SDS. Membranes were blocked for 2 h at room temperature in TBSTw (10 mM Tris–HCl, pH 8.0, 150 mM NaCl, 0.2% Tween-20) containing 5% non-fat milk powder, briefly rinsed in TBSTw, and then incubated overnight at 4 °C with polyclonal anti-ZONAB or monoclonal anti-ZO-2 antibody in TBSTw containing 1% non-fat milk powder. Membranes were then washed in TBSTw for 40 min, incubated with horseradish peroxidase-conjugated donkey anti-rabbit or anti-mouse IgG diluted 1:3000–1:5000 (Sigma-Aldrich Canada, Oakville, Ontario, Canada) in TBSTw containing 1% non-fat milk powder, washed in TBST (Tris–HCl, pH 7.4, containing 1.5% NaCl, 0.3% Triton X-100) for 40 min and resolved by chemiluminescence (ECL, Amersham PB, Baie d'Urfe, Quebec, Canada).

Co-IP of Cx36 and ZO-2

IP of ZO-2 from mouse retina was conducted as previously described (Li et al., 2004a,b). Briefly, mouse retinas were homogenized in IP buffer, the homogenate was sonicated and centrifuged, and 500 μg of supernatant protein was pre-cleared by incubation with 20 μl of protein-A agarose beads for 1 h at 4 °C. The beads were then incubated with 2 μg of monoclonal anti-ZO-2 antibody for 16 h at 4 °C, followed by 1 h incubation with 20 μl of protein-A agarose beads. The mixture was centrifuged at 20,000×*g* for 10 min, and the beads were washed five times in 1 ml of buffer (20 mM Tris–HCl pH 8.0, 150 mM NaCl, and 0.5% NP-40). After incubation for 2 min at 60 °C in 20 μl of SDS-PAGE loading buffer, the samples were subjected to SDS-PAGE and immunoblots were probed with polyclonal anti-Cx36 antibody 51-6300.

Light microscope immunohistochemistry

Mice deeply anesthetized with equithesin (3 ml/kg) (Scadding, 1981) were transcardially perfused with 3 ml of cold “pre-fixative” solution (50 mM sodium phosphate buffer, pH 7.4, 0.9% NaCl, 0.1 sodium nitrate and 1 unit/ml heparin). This was followed by perfusion with 40 ml of cold 0.16 M sodium phosphate buffer, pH 7.6, containing either 1% or 2% formaldehyde and 0.2% picric acid. Animals were then perfused with 10 ml of 25 mM sodium phosphate buffer, pH 7.4, containing 10% sucrose. After removal, eyes were stored at 4 °C for 24–72 h in cryoprotectant consisting of the final perfusate with addition of 0.04% sodium azide. Vertical sections of retina were cut at a thickness of 10 μm on a cryostat, and collected on gelatinized glass slides. All sections were washed for 20 min in 50 mM Tris–HCl, pH 7.4, containing 256 mM sodium chloride (TBS) and 0.3% Triton X-100 (TBSTr). Primary antibodies were diluted in TBSTr containing 5% or 10% normal goat or normal donkey serum.

For single immunofluorescence labeling, sections were incubated for 24 h at 4 °C with either monoclonal or polyclonal anti-Cx36, anti-ZO-1, ZO-2, polyclonal anti-ZONAB or polyclonal anti-calretinin, then washed for 1 h in TBSTr, and incubated with secondary antibodies for 1.5 h at room temperature. Various secondary antibodies used included fluorescein isothiocyanate-conjugated horse anti-mouse IgG diluted 1:100 (Vector Laboratories, Burlingame, CA, USA), Cy3-conjugated goat anti-mouse IgG diluted 1:200 (Jackson ImmunoResearch Laboratories, West Grove, PA, USA), Alexa Fluor 488-conjugated goat anti-rabbit IgG diluted 1:1000 (Molecular Probes, Eugene, OR, USA), Cy3-conjugated donkey anti-rabbit diluted 1:200 (Jackson ImmunoResearch Laboratories), and Alexa Fluor 488-conjugated donkey anti-goat IgG diluted 1:1000 (Molecular Probes). Sections used for single labeling with anti-Cx36, anti-ZONAB, anti-ZO-1 and anti-ZO-2 were counterstained with either red Nissl fluorescent NeuroTrace (stain N21482) or green Nissl NeuroTrace (stain N21480) (Molecular Probes).

For double immunofluorescence labeling involving Cx36, sections were incubated as above with monoclonal anti-Cx36 antibodies and simultaneously with one of the following antibodies: polyclonal anti-ZO-1, polyclonal anti-ZONAB or polyclonal anti-calretinin. Conversely, polyclonal anti-Cx36 was incubated simultaneously with monoclonal anti-ZO-1. For double-labeling involving ZO-1, sections were incubated with monoclonal anti-ZO-1 and simultaneously with either polyclonal anti-ZONAB or polyclonal anti-calretinin. For double-labeling involving ZO-2, sections were incubated with monoclonal anti-ZO-2 and simultaneously with either polyclonal anti-Cx36, polyclonal anti-ZO-1 or polyclonal anti-ZONAB. For double-labeling involving ZONAB, sections were incubated with rabbit polyclonal anti-ZONAB and simultaneously with goat polyclonal anti-calretinin. For triple immunofluorescence labeling, sections were incubated simultaneously with combinations of antibodies against the following: Cx36, ZO-1 and calretinin; Cx36, ZONAB and calretinin; or ZONAB, ZO-1 and calretinin. Primary antibody incubations were followed by washes in TBSTr for 1 h at room temperature, and then incubations for 1.5 h at room temperature simultaneously with AlexaFlour 488-conjugated donkey anti-goat IgG diluted 1:1000, Cy3-conjugated donkey anti-rabbit IgG diluted 1:200 and Cy5-conjugated goat anti-mouse IgG diluted 1:200. After secondary antibody incubations, all sections were washed in TBSTr for 20 min, and then in 50 mM Tris–HCl buffer, pH 7.4, for 30 min. Sections were covered with antifade medium and coverslipped. Control procedures were performed for each of the antibody combinations used and included omission of one of the primary antibodies with inclusion of each of the secondary antibodies for each combination of labeling to establish absence of inappropriate cross-reactions between primary and secondary antibodies or between different combinations of secondary antibodies.

Confocal microscopy

Fluorescence was examined on a Zeiss Axioskop2 fluorescence microscope with image capture using a 60× objective lens and Axiovision 3.0 software (Carl Zeiss Canada, Toronto, Ontario, Canada). Confocal immunofluorescence analyses of double and triple labeling was performed on an Olympus Fluoview IX70 confocal microscope with image capture using Olympus Fluoview software. Images were assembled according to appropriate size and contrast using Adobe Photoshop CS (Adobe Systems, San Jose, CA, USA), Corel Draw 12, and Northern Eclipse software (Empix Imaging, Mississauga, ON, Canada). Confocal images were acquired either as single scans or as stacks of five consecutive scans in the *z* axis of randomly chosen fields in retinal inner plexiform layer (IPL) or outer plexiform layer (OPL) layers. Stacks of scans were taken at *z* axis intervals of either 1 μm (as in Fig. 3A-C), or at 0.4 μm (as in Fig. 4G-L). The large scan interval with stacks of five scans in Fig. 3 provided a greater depth of tissue, and thereby a larger number of puncta for each of the proteins illustrated, and demonstrates the relative densities of these puncta in sublaminar regions of the IPL, which is often not evident in single scans of the same proteins. To a limited extent, observations of co-

localized punctate labeling of proteins in such stack may occur artifactually by overlap of non-co-localized labeling in different planes. Therefore, rotation of stack images (as in Fig. 3A-C) allowed determination of artifactual co-localization, which occurred in only a small number of apparently co-localized puncta, and most overlapping puncta were confirmed to represent true co-localization. Nevertheless, in addition to presentation of results in stacked images, some observations are also presented as single scans. As well, FRIL analysis (described below) was used to confirm ultrastructural co-localization. Quantitative analysis of co-localization between Cx36/ZO-1, Cx36/ZONAB and ZONAB/ZO-1 was conducted using the single confocal scans that are presented as stacked images in Fig. 3A-C. Quantitative analysis of ZO-2 co-localization with Cx36, ZONAB and ZO-1 was conducted using single confocal scans of six separate randomly selected fields of the IPL from two to three mice. Values are presented as percentage of Cx36-positive puncta that were positive for ZO-1 and ZONAB, percentage of ZONAB-positive puncta that were positive for ZO-1, and percentage of ZO-2-positive puncta that were positive for Cx36, ZONAB and ZO-1.

FRIL electron microscopy

Two adult Sprague–Dawley rats (one male, one female) were fixed by whole-body perfusion with 2% formaldehyde, the eyes were removed, and 150 μm thick slices of retina were obtained with a Lancer 1000 refrigerated Vibratome. Tissue slices were infiltrated with 30% glycerol as cryoprotectant, frozen by rapid contact with a liquid-nitrogen-cooled copper mirror, fractured and replicated in a JEOL 9010c freeze-fracture device (RMC Products, Tucson, AZ, USA), and while still frozen, stabilized in Lexan plastic on a gold “index” TEM grid, as previously described (Rash and Yasumura, 1999). Samples were thawed, photomapped by confocal microscopy, cleaned of bulk tissue remnants by washing for 29 h in 2.5% SDS detergent (Fujimoto, 1995). One replica was double-labeled by immunogold using mouse monoclonal antibody Ab37-4600 against Cx36 and rabbit polyclonal antibody against ZO-1 (Ab61-7300), two replicas were double-labeled using rabbit polyclonal antibody 36-4600 against Cx36 and mouse monoclonal antibody Ab611561 against ZO-2, one replica was single-labeled with anti-ZO-1 Ab61-7300, and one replica was double-labeled with monoclonal anti-Cx36 and polyclonal anti-ZONAB. Replicas were counter-labeled with goat anti-mouse (12 nm gold beads) and goat anti-rabbit (six and 18 nm gold beads) (Jackson ImmunoResearch Laboratories). Labeled replicas were rinsed, air dried, coated on the labeled side with 10–20 nm of carbon (to stabilize gold labels and to anneal cracks in the replica), and examined in JEOL 2000 EX-II or JEOL 1200 EX TEMs operated at 100 kV. Images were photographed as stereo pairs (8° included angle), digitized using an ArtixScan 2000f digital scanning device, and prepared using Photoshop 7.01 (Adobe systems). FRIL images are presented as stereoscopic pairs, or as stereoscopic triplets, with the intaglio (or reverse stereoscopic) image considered to be essential for recognizing 6 nm gold beads on the electron-opaque platinum/carbon replica.

RESULTS

Cx36, ZO-1 and ZONAB in mouse retina

The general distributions of Cx36, ZO-1, ZO-2 and ZONAB were compared in low magnification images of vertical retinal sections from CD1 mice labeled for each of these proteins by immunofluorescence and simultaneously counterstained with Nissl fluorescent Neurotrace (Fig. 1). Immunolabeling consisted of fluorescent puncta, as well as continuous labeling of ZO-1 and ZO-2 along blood vessels (Fig. 1C, E), which was more evident for ZO-1 than ZO-2. Intense labeling of ZO-1, ZO-2 and ZONAB was also present at the outer limiting membrane (OLM), which was consistent with previous findings in the case of ZO-1 and ZO-2 (Williams and Rizzolo, 1997;Tserentsoodol et al., 1998;Collins and Rizzolo, 1998).

Labeling for Cx36 was restricted to the IPL and OPL, and was very dense in the inner half of the IPL, often obscuring visualization of individual puncta at low magnification (Fig. 1A). Labeling for ZO-1 was of moderate density throughout the IPL, except in a narrow band in the middle of this layer, where it was of slightly higher density (Fig. 1C). Punctate labeling for ZO-1 was also evident in OPL, but was partly obscured by ZO-1-positive blood vessels in this layer (Fig. 1C). Within the main retinal layers, punctate labeling for ZO-2 was restricted to the IPL, where it was more sparse than the other proteins examined, but was particularly conspicuous in the outer region of the IPL (Fig. 1E). Anti-ZO-2 antibodies from both BD Biosciences (Fig. 1E) and Invitrogen/Zymed (not shown) produced similar labeling in retina. In addition to punctate labeling in the IPL, these antibodies generated against different non-overlapping sequences in ZO-2 both gave immunoreactivity associated with neuronal nucleoli in the ganglion cell layer and inner nuclear layer (INL), the significance of which remains uncertain. Labeling for ZONAB was restricted to the plexiform layers and was characterized by dispersed ZONAB-positive puncta in the IPL and a continuous band of puncta in the OPL (Fig. 1G). In the IPL, ZONAB tended to be more concentrated in the outer and inner third than in the middle third of this layer (Fig. 1G).

ZONAB and ZO-2 antibody characterization

Detection of ZONAB with anti-ZONAB antibody was confirmed using HeLa cells transiently transfected with an expression vector containing the short ZONAB A isoform. By immunofluorescence, transfected cells displayed punctate labeling around their periphery (Fig. 2A), while empty vector-transfected cells were devoid of labeling (Fig. 2B). In immunoblots (using 12.5% gels) of HeLa cells transfected with ZONAB, anti-ZONAB detected a band migrating at approximately 31 kDa (Fig. 2C, lane 1), which was very close to the predicted molecular weight of the ZONAB A (MSY3) alternatively spliced short isoform (30.7 kDa). A protein of unknown identity was detected at about 28 kDa in both ZONAB-transfected and empty vector-transfected cells (Fig. 2C, lanes 1 and 2). Since HeLa cells are of human origin, the additional band detected in these cells does not detract from the specificity of the anti-ZONAB antibody for detection of ZONAB in mouse retina. It is also noteworthy that despite the anomalous band detected in both control and ZONAB-transfected cells, no immunofluorescence labeling for ZONAB was seen in control nontransfected HeLa cells (Fig. 2B). In immunoblots using 10% gels, a 31 kDA band was also detected in homogenates of retina (Fig. 2D, lane 1), and this band corresponded to the 31 kDa band seen in ZONAB-transfected HeLa cells (Fig. 2D, lane 2). The longer alternatively spliced form of ZONAB, ZONAB B, with predicted molecular weight of 38.8 kDa, was not detected in either retina or HeLa cells.

Cx36 association with ZO-2

Detection of ZO-2 in mouse retina and its co-association with Cx36 in this tissue was confirmed by Western blotting. Anti-ZO-2 antibody 71-1400 recognized a band migrating at 160 kDa (Fig. 2E), corresponding to the molecular weight of ZO-2. IP of ZO-2 from homogenates of retina using antibody 611561 resulted in detection of a protein band in the immunoprecipitate that was identified as Cx36 by its molecular weight (Fig. 2F, lane 2) and its co-migration with Cx36 detected in homogenate of retina (Fig. 2F, lane 1). A control lane loaded with IP material after omission of anti-ZO-2 antibody during the IP procedure showed an absence of Cx36 detection (Fig. 2F, lane 3).

Confocal microscopy of Cx36, ZO-1 and ZONAB

Double immunofluorescence confocal microscopy was used to examine sublaminar distributions and co-localization relationships of Cx36, ZO-1 and ZONAB in vertical sections through the IPL of retina from CD1 mice. Each of the images in Fig. 3A-C represents z-stacks

of five scans, which were taken to provide an enrichment of labeling compared with that seen in single scans, thereby allowing a greater appreciation of the relative distributions and organization of punctate labeling for the proteins within sub-regions of the IPL. Cx36-positive puncta in the inner half of IPL were of larger size on average than those in the outer half of IPL, which may have contributed to the appearance of a greater intensity of labeling for Cx36 in the inner half seen in Fig. 1A. In addition, small aggregates of Cx36-positive puncta were occasionally seen along a thin band in the mid-region of IPL, and this region was flanked by avenues of sparse labeling for Cx36, with the upper avenue evident in Fig. 3A1 and 3B1, and the lower one better seen in Fig. 3A1. Labeling for ZO-1 appeared as puncta of more uniform size and generally of finer grain (Fig. 3A2, 3C2) compared with Cx36-positive puncta. As in the case of Cx36, small aggregates of ZO-1-positive puncta were seen in the mid-region of the IPL, below which was located a strip of sparse labeling (Fig. 3A2). Counts of co-localized puncta in image overlays of double immunofluorescence labeling for Cx36 and ZO-1 in single scans indicated that the majority of Cx36-positive puncta were labeled for ZO-1 (Table 2), whereas many ZO-1-positive puncta were not labeled for Cx36. Labeling of ZO-1-puncta alone was evident in the inner and more so in the outer half of IPL (Fig. 3A3). Results of double labeling with monoclonal anti-Cx36 Ab37-4600 and polyclonal anti-ZO-1 Ab61-7300 (Fig. 3A) were similar to that obtained with polyclonal anti-Cx36 Ab36-4600 and monoclonal anti-ZO-1 Ab33-9100 (not shown).

Features of ZONAB distribution (Fig. 3B2) included sparse labeling within the extreme inner region of IPL, with increasing density toward a band almost devoid of ZONAB, corresponding to a band nearly devoid of Cx36 (Fig. 3B1). Beyond this band in the outer region of IPL, ZONAB-positive puncta were concentrated along a narrow strip, and most of these puncta was distinctly larger in size than most of the other ZONAB-positive puncta observed in the IPL (Fig. 3B2). Double labeling indicated a high degree of Cx36 and ZONAB co-localization in mid-regions of the IPL, as well as within the band containing large ZONAB-positive puncta (Fig. 3B3). Cx36-positive puncta devoid of labeling for ZONAB were most concentrated in the extreme inner part of IPL, whereas ZONAB-positive puncta lacking Cx36 were most concentrated in the extreme outer part of the IPL (Fig. 3B3). Counts of puncta in single scans revealed that 39% of Cx36-puncta were positive for ZONAB. Double labeling showed that a proportion of ZONAB-positive puncta (44%; Table 2) was also labeled for ZO-1, whereas many ZO-1-positive puncta, particularly in the mid-region of IPL containing a greater density of ZO-1, were devoid of labeling for ZONAB (Fig. 3C). The laminar distributions and co-localization of Cx36, ZO-1 and ZONAB described above in retina of CD1 mice were similarly observed in rat retina (not shown).

Detailed analyses of ZO-1 in relation to Cx36 in the OPL indicated that the vast majority of Cx36-positive puncta in the OPL was co-localized with ZO-1 (Ciolofan et al., unpublished observations). Confocal double immunofluorescence revealed that most of the punctate labeling of Cx36 in the OPL was also associated with ZONAB (Fig. 3D, shown only in overlay). Compared with the moderate density of ZONAB-positive puncta in the OPL of retina from WT mice (Fig. 3E), there was a substantial reduction of labeling for ZONAB in the OPL of retina from Cx36 KO mice (Fig. 3F).

ZO-1 and ZONAB in the IPL of retina from Cx36 KO mice

Low magnifications of immunolabeling for ZO-2 and ZONAB in retina of Cx36 KO mice are shown in Fig. 3G and 3H, respectively. In addition, double confocal immunofluorescence was used to examine expression and labeling patterns of ZO-1 and ZONAB in the IPL of retina from Cx36 KO mice. Because Cx36 gene deletion was achieved in the C57BL6/129SvEv hybrid mouse strain (Deans et al., 2001), we confirmed that the distributions, relative densities and co-localization relationships of Cx36/ZO-1 (Fig. 4A), Cx36/ZONAB (Fig. 4C) and ZO-1/

ZONAB (Fig. 4E) in the IPL of WT C57BL6/129SvEv mice paralleled that described above in retina of CD1 mice (Fig. 3A-C). In addition, the co-localization relationships observed in the Z-stacks shown in Fig. 3A-C were confirmed using the single confocal scans in Fig. 4A, C and E. As presented in overlay images, double immunofluorescence of Cx36 and ZO-1 in the IPL of retina from Cx36 KO mice showed an absence of Cx36 (green) labeling and slightly reduced ZO-1 (red) expression (Fig. 4B). Double-labeling of Cx36 and ZONAB in retina of Cx36 KO mice showed that the absence of Cx36 (green) in the IPL resulted in a large reduction of ZONAB (red) in the inner two thirds of the IPL (Fig. 4D). However, the band of large ZONAB-positive puncta in the outer one-third region of the IPL was still present (Fig. 4D) and appeared similar to that observed in WT mice. Double-labeling of ZONAB (green) and ZO-1 (red) in retina of Cx36 KO mice showed less ZO-1/ZONAB co-localization in the inner two-thirds of the IPL due to reduced labeling of ZONAB in this region (Fig. 4F). However, ZO-1/ZONAB co-localization was largely preserved in the outer third of the IPL (Fig. 4F).

Confocal microscopy of ZO-2 with Cx36, ZONAB and ZO-1

Double immunofluorescence confocal analyses of ZO-2 in relation to Cx36, ZONAB and ZO-1 in the IPL of WT and Cx36 KO C57BL6 mice are shown in Fig. 4G-L, where images represent z-stacks of five scans. In the IPL of WT mice, ZO-2-immunopositive puncta were consistently of lower density than that of punctate labeling for Cx36, ZO-1 or ZONAB, although labeling of the latter proteins in this set of samples was somewhat less robust than typically observed. Nevertheless, both anti-ZO-2 Ab71-1400 (not shown) and Ab611561 revealed that nearly all ZO-2-puncta were immunopositive for Cx36 (Fig. 4G) as well as for ZONAB (Fig. 4I), and most were positive for ZO-1 (Fig. 4K). Relatively large prominent ZO-2-puncta located in the outer portion of the IPL were especially conspicuous with respect to their co-labeling with Cx36, ZONAB and ZO-1. As shown in Table 2, counts of puncta in single scans indicated that a high percentage of ZO-2-puncta was co-localized with Cx36, ZONAB and ZO-1. As expected based on the relatively lower density of labeling for ZO-2 compared with the other proteins, only a subset (29%) of punctate labeling for Cx36 was immunopositive for ZO-2, and subsets of ZO-1 and ZONAB were positive for ZO-2 (not examined quantitatively). In retina of Cx36 KO mice, with results shown only by overlay of double labeling, ZO-2-puncta were markedly decreased in the inner IPL, but remained in the outer IPL (Fig. 4H, green). As already described above, immunoreactivity of Cx36 was eliminated (Fig. 4H, red), labeling of ZONAB was largely reduced in the inner part of IPL, but persisted in the outer IPL (Fig. 4J, red), and labeling of ZO-1 was slightly reduced (Fig. 4L, red). Punctate labeling that persisted in the outer part of IPL in Cx36 KO mice consistently exhibited ZO-2/ZONAB co-localization (Fig. 4J, green/red, respectively), as well as ZO-2/ZO-1 co-localization (Fig. 4L, green/red, respectively).

Despite the above observations indicating reductions of ZONAB and ZO-2 immunolabeling in the inner part of the IPL of Cx36 KO retina, we were unable to detect reductions of these proteins in retinas from Cx36 KO mice. This may be due partly to the persistence of ZO-2 and ZONAB in outer part of the IPL of Cx36 KO retina and, perhaps more so, to the high concentration of these proteins in the retinal OLM of both WT (Fig. 1E, G) and Cx36 KO mice (Fig. 3G, H).

Cx36, ZO-1 and ZONAB in relation to calretinin in IPL

To assign a precise location of Cx36/ZO-1/ZO-2/ZONAB-positive puncta that remain positive for ZO-1/ZO-2/ZONAB in the IPL of Cx36 KO mice, labeling of these proteins was examined in vertical sections of retina that were simultaneously labeled for calretinin. This was achieved by triple labeling for Cx36, ZO-1 and calretinin in WT mice, shown at low (Fig. 5A) and at higher confocal magnification (Fig. 5B), and by triple labeling for ZONAB, ZO-1 and calretinin in WT mice (Fig. 5C) and double labeling for ZONAB and calretinin in Cx36 KO mice (Fig. 5D). Calretinin has been well documented as a marker of subclasses of amacrine cells with

somata lying within the inner edge of the INL, and displaced amacrine cells located in the ganglion cell layer (Jeon and Jeon, 1998). These two subclasses of cells have a characteristic trilaminar distribution pattern of dendritic processes in the middle to outer half of the IPL (Fig. 5A3). Triple labeling revealed that Cx36 (Fig. 5A1, A4) and ZO-1 (Fig. 5A2, A5) were distributed sparsely along the inner calretinin-positive band, moderately in the region between the outer two calretinin-positive bands, and abundantly in a region between the inner two calretinin bands. Magnified confocal images showed a high degree of Cx36/ZO-1 co-localization in the IPL sublamina encompassed by the calretinin-positive bands, including those puncta between the outer two bands (Fig. 5B). Triple labeling in WT mice showed a similar distribution of ZONAB in relation to calretinin (Fig. 5C1) as observed in the case of Cx36 and ZO-1, and indicated substantial co-localization of the larger ZONAB-positive puncta with ZO-1 in the region between the outer two calretinin-positive bands (Fig. 5C2). Double labeling for ZONAB and calretinin in retina of Cx36 KO mice revealed that labeling for ZONAB persisting in the IPL of these mice was located between the two outer calretinin bands and partially overlapped the outer band (Fig. 5D).

FRIL of Cx36, ZO-1, ZO-2 and ZONAB in retina

ZO-2 and Cx36 co-localized at gap junctions—At low magnification, immunogold beads indicating labeling for Cx36 and for ZO-2 revealed the locations of gap junctions throughout the IPL. Of 37 gap junctions detected in one replica, 29 contained gold beads for Cx36 only (78%; not shown), eight (22%) were double-labeled for Cx36 plus ZO-2 (Fig. 6), and none (0%) were found to be labeled for ZO-2 without co-labeling for Cx36. In this replica, Cx36 was labeled by 12-nm gold beads and ZO-2 was labeled by both 6-nm and 18-nm gold beads. Double-labeled gap junctions included conventional “plaque” gap junctions (Fig. 6A-B), as well as “reticular” (Fig. 6C) and “string” gap junctions (Fig. 6D). Morphological types of gap junctions are defined and illustrated in Rash et al. (2004).

ZO-1 in non-gap junctional membrane specializations—Consistent with immunofluorescence observations (Fig. 1C), FRIL revealed immunogold labeling of ZO-1 (Fig. 7A-B) at the level of the OLM. By thin section electron microscopy (not shown), the OLM is seen to consist of desmosome-like adherens junctions and their “terminal web” of cytoplasmic filaments in photoreceptors and in the Müller cell “collars” that surround each photoreceptor. [In rats, which are nocturnal animals, ca. 99% of photoreceptors are rods and ca. 1% are cones (LaVail, 1976), so we designate these cells generically as rods.] In low magnification FRIL images (Fig. 7A), the OLM region is detected as a narrowing of adjacent rods between the rod inner segments (RIS) and rod outer segments (ROS). Bands of immunogold beads for ZO-1 were confined to the constricted regions. Moreover, the immunogold beads were concentrated within the rod cytoplasm (directly beneath rod P-faces), thereby documenting freeze-fracture labeling of sub-plasma membrane cytoplasmic constituents (Fig. 7A). In addition, equally abundant gold beads for ZO-1 were present within the Müller cell cytoplasm (Fig. 7B) at the level of the Müller cell “collar” that surrounds, adheres to, and constricts the rod initial shaft. Although neither gap junctions nor tight junctions were found at the OLM, adherens junctions are present at the OLM, providing further corroboration that ZO-1 is localized to a third type of inter-cellular junction (i.e. adherens junctions) formed along the apical and lateral surfaces of neurons and epithelial cells.

Immunogold labeling for ZO-1 also was found beneath clusters of P-face intramembrane particles (IMPs) of both presynaptic active zones (not shown) and post-synaptic densities (PSDs) (Fig. 7C), including at least one type of non-glutamate receptor PSD. However, gold beads were not detected beneath the E-face IMPs that are characteristic of glutamate receptors (Fig. 7C, arrowhead). (For ultrastructural and FRIL identifications of glutamate receptors, see Harris and Landis, 1986;Pereda et al., 2003a,b,2004;Rash et al., 2004). It should be noted that

E-face IMPs represent transmembrane proteins that have been separated from their associated cytoplasmic accessory proteins and then replicated on their cytoplasmic surfaces. Consequently, cytoplasmic accessory proteins like ZO-1 would necessarily be separated from all classes of E-face IMPs, and hence, could not be labeled there, even if present prior to fracture.

Cx36 and ZONAB in ultrastructurally-defined gap junctions—In one sample that was double-labeled for Cx36 plus ZONAB, 31 gap junctions were detected, 18 of which were single-labeled for Cx36 (Fig. 8A), five were double-labeled for Cx36 plus ZONAB (Fig. 8B-C), five were single-labeled for ZONAB (Fig. 8D), and three were unlabeled (not shown). In all cases, Cx36 labeling was relatively weak (LE=1:100), suggesting that the primary or secondary antibody to Cx36 had lost potency. In contrast, the level of labeling for ZONAB at some gap junctions was equal to the highest labeling for Cx36 in our previous replicas, and much higher than labeling for ZO-1 or ZO-2, to which it is presumably bound. This also suggests that the ZONAB antibody is particularly useful for FRIL. Finally, we know that by FRIL, ZONAB was not detected in PSDs or in Müller cell gap junctions. Efforts are under way to determine by FRIL if immunogold labeling for ZONAB occurs at contacts of Müller cells with rods or cones at the OLM.

DISCUSSION

This report demonstrates by LM and FRIL that Cx36, ZO-1, ZO-2, and ZONAB are co-localized at a significant fraction of interneuronal gap junctions in the IPL of retina. ZONAB, a nucleic acid binding and regulatory protein, is an intra-cellular signaling molecule that may be involved in suppression or activation of gene transcription in response to functional alterations of adjacent cells linked by tight junctions, gap junctions, and/or adherens junctions (Balda and Matter, 2003; Li et al., 2003). Thus, determining the precise subcellular locations and activities of these accessory proteins is essential for understanding how their distributions and associations with cell–cell junctions, including retinal gap junctions, contribute to cellular homeostasis.

Cx36 at retinal gap junctions

Our LM observations of Cx36 distribution in mouse retina are consistent with results in numerous reports on this Cx in retina of various species. To date, dense labeling of Cx36 observed in the inner half of IPL has been ascribed to Cx36 in dendrites of AII amacrine cells and ON-alpha ganglion cells (Feigenspan et al., 2001; Mills et al., 2001; Hidaka et al., 2004; Schubert et al., 2005). In this region, there is evidence for the presence of Cx36 in gap junctions between homologously coupled AII amacrine cells, between AII amacrine cells heterotypically coupled with ON-cone bipolar cell axon terminals that lack Cx36, and between ON-alpha ganglion cells heterotypically coupled with wide-field amacrine cells that apparently do not express Cx36 (Famiglietti and Kolb, 1975; Strettoi et al., 1992; Güldenagel et al., 2001; Feigenspan et al., 2001; Mills et al., 2001; Deans et al., 2002; Schubert et al., 2005). Moderate labeling of Cx36 in the outer half of IPL has been ascribed to Cx36 in OFF-alpha ganglion cell dendrites, forming homologous gap junctions with each other and heterologous gap junction with dendrites of wide-field amacrine cells (Hidaka et al., 2004; Schubert et al., 2005). Somewhat more sparse labeling of Cx36 in the OPL has been assigned to Cx36 expression in cone pedicles and OFF-cone bipolar cell dendrites (Lee et al., 2003; Feigenspan et al., 2004).

ZO-2 at gap junctions in mouse retina

Like ZO-1, ZO-2 is a well-established MAGUK (membrane-associated, guanylate kinase-like) protein, and was reported to be associated with both tight junctions and adherens junctions (Itoh et al., 1999a,b; González-Mariscal et al., 2000, 2003). Direct molecular interaction of

ZO-1 with ZO-2 has been demonstrated to occur via the second PDZ domains in each of these proteins (González-Mariscal et al., 2000, 2003). Although ZO-2 has not been reported to be widely associated with gap junctions, it was co-localized with Cx32 in hepatocytes (Kojima et al., 2001) and was found to interact with the c-terminus of Cx43 (Singh and Lampe, 2003; Singh et al., 2005). Our results demonstrate localization of ZO-2 at gap junctions and, in particular, at a subpopulation of those junctions containing Cx36 and ZO-1 in rodent retina. Whether ZO-2 at these gap junctions directly interacts with Cx36, with ZO-1 or some other protein requires further molecular analysis. However, the present results showing co-IP of ZO-2 with Cx36 suggest that these proteins interact. In addition, it is noteworthy that Cx36 interaction with the first PDZ domain of ZO-1 occurs via a YV binding motif present at the carboxy-terminus of the Cx36 sequence (Li et al., 2004a), and this same YV binding motif is present in the claudin family of proteins, which directly interacts with the first PDZ domains of both ZO-1 and ZO-2 (Itoh et al., 1999b). Thus, sequence analysis and the current immunocytochemical data suggest that Cx36 may directly interact with ZO-2 at retinal gap junctions. Confirmation of this hypothesis will require analysis by molecular approaches.

Previous studies have shown expression of ZO-1 and ZO-2 in retina only at the OLM (Collins and Rizzolo, 1998; Paffenholz et al., 1999; Inoko et al., 2003). This was confirmed by immunofluorescence as well as by FRIL, which revealed ZO-1 to occur in the OLM in the absence of gap junctions or tight junctions. However, a wider distribution of ZO-2 in retina was found in the present study, using two different antibodies directed against different epitopes in the ZO-2 sequence. Detection of ZO-2 in additional locations may be attributed to our use of weak tissue fixation conditions, which appear to be required for adequate immunocytochemical detection of ZO-1 and ZO-2 MAGUK proteins in neural tissues (Li et al., 2004a; Penes et al., 2005). The ZO-2-positive puncta that we detected in the IPL were highly co-localized with Cx36, indicating neuronal expression of ZO-2 since Cx36 is expressed exclusively by neurons in retina. In addition, ZO-2 was found in ultrastructurally-defined gap junctions by FRIL. However, both by LM and EM, it was clear that only a subpopulation of Cx36-expressing neurons also contains ZO-2, and the identity of these neurons remains to be determined.

ZO-1 and ZONAB at retinal gap junctions

Although classically considered a tight junction-associated protein, identification of ZO-1 association with gap junctions composed of a variety of different connexins has raised the possibility that additional accessory or scaffolding proteins similar to those associated with ZO-1 at tight junctions (González-Mariscal et al., 2003) may also be anchored by ZO-1 at gap junctions. Among such proteins, we chose to examine ZONAB, which was previously shown to interact with ZO-1 at tight junctions of cultured MDCK cells (Balda and Matter, 2000; Balda et al., 2003). Our results demonstrated ZONAB expression in mouse and rat retina, and substantial ZONAB co-localization with both Cx36 and ZO-1 in the IPL, as well as of ZO-1 with ZONAB, indicating the co-association of all three proteins at individual puncta. This was confirmed by FRIL, which showed ultrastructural co-localization at confirmed neuronal gap junctions. Similarly, we have reported elsewhere that Cx36 associated with rod spherules in the OPL was nearly totally co-localized with ZO-1 (Ciolofan et al., unpublished observations). These results, together with the substantial Cx36/ZONAB overlap observed presently in the OPL, indicate that co-association of Cx36/ZO-1/ZONAB also occurs in the OPL of retina. It is noteworthy that another major connexin present in the OPL, namely Cx57, showed a total lack of co-localization with either ZO-1 (Ciolofan et al., unpublished observations) or with ZONAB (not shown), consistent with the lack of Cx57 co-localization with Cx36, indicating selectivity of ZO-1/ZONAB association with retinal Cx36.

Together with previous FRIL studies demonstrating the presence and co-localization of Cx36 and ZO-1 in individual gap junctions between retinal neurons (Li et al., 2004a; Rash et al., 2004), ZONAB also is now shown to be a component of a subpopulation of neuronal gap junctions containing Cx36 in retina. This may reflect selectivity of ZONAB expression in only a subpopulation of neurons that express Cx36, or alternatively, localization of ZONAB at only a portion of Cx36-containing gap junctions in individual neurons. Conversely, as in the case of many ZO-1-puncta lacking Cx36, not all ZONAB was associated with either Cx36 or with ZO-1, indicating the presence of ZONAB and ZO-1 in as-yet-unidentified punctate structures lacking Cx36. By FRIL, approximately 10% of these were identified as neuronal gap junctions without detectable Cx36. From previous data on gap junctions comprised primarily or exclusively of Cx45 without Cx36, it is noteworthy that Cx45 in the IPL exhibited a total lack of co-localization with ZONAB (unpublished observations), indicating association of ZONAB with a specific subclass of retinal neuronal gap junctions composed of Cx36, and lacking Cx45, in the IPL.

Following its recent identification, only a few reports have appeared on ZONAB or its mouse ortholog, which has also been referred to as MsY3 (ZONAB A) for the short isoform and MsY4 for the long isoform (ZONAB B). ZONAB was found to be expressed in brain, heart, spleen, liver and muscle, with the highest levels observed in testis (Mastrangelo and Kleene, 2000; Davies et al., 2000). This transcription factor was reported to cause translational repression of protamine-1 mRNA in spermatids (Giorgini et al., 2001, 2002) and transcriptional repression of the tyrosine kinase receptor ErbB2 (Neu or HER2) in canine MDCK cells (Balda and Matter, 2000; Balda et al., 2003). In MDCK cells, ZONAB was shown to interact with the SH3 domain of ZO-1, and it was suggested that sequestration of ZONAB by ZO-1 at tight junctions derepresses ErbB2 expression, thereby promoting ErbB2-mediated cell differentiation (Balda and Matter, 2000; Balda et al., 2003). It is noteworthy that neuregulins act as ligands for the ErbB2 receptor, and that neuroregulin/ErbB2 signaling is essential for a variety of cellular processes, such as cell growth and differentiation (Casalini et al., 2004; Holbro and Hynes, 2004; Marmor et al., 2004). Both ErbB2 and neuregulin were found to be expressed in mammalian retina, and neuregulin was reported to promote the survival and neurite extension of retinal neurons (Bermingham-McDonogh et al., 1996; Williams et al., 1998; Lindqvist et al., 2002). Thus, we speculate that ZO-1/ZONAB may participate in local regulatory control of retinal gap junctions and contribute to far reaching regulatory processes involved in retinal function and development. Such processes may be dependent on ZO-1/ZONAB targeting to and/or release from gap junctions in order to control the transcriptional functions of ZONAB at such genes as ErbB2. However, further biochemical and molecular studies are required to establish ZO-1/ZONAB interaction in retina and to determine transcriptional activities of ZONAB in retinal neurons.

ZO-1, ZO-2 and ZONAB in Cx36 KO retina

Besides co-localization of ZO-2 and ZONAB with Cx36 in retina of WT mice, the large reductions of ZO-2 and ZONAB that we observed in the inner part of the IPL in Cx36 KO mice provide additional support for the association of these two proteins with gap junctions by showing the requirement of Cx36 for their stable expression and subcellular targeting. The modest reductions of ZO-1 observed in the IPL of Cx36 KO mice (see also Li et al., 2004a) may be explained by the presence of many ZO-1-puncta in this layer that were not associated with Cx36 and that remained unaffected by Cx36 gene deletion. Curiously, despite association of Cx36 with a band of large punctate labeling for ZO-1, ZO-2 and ZONAB in the outer part of the IPL, the relative amount of labeling of these latter proteins along this band was unaffected by the absence of Cx36.

The spatial distributions of Cx36, ZO-1 and ZONAB in the IPL were determined in relation to calretinin-positive cell processes (blue bands in Fig. 5), which allowed precise localization of the punctate labeling for ZO-1, ZO-2 and ZONAB that remains in Cx36 KO retina. Immunocytochemical markers for AII amacrine cells include the use of parvalbumin or calretinin in retinas of various species (Gabriel and Straznicky, 1992;Wässle et al., 1993, 1995;Casini et al., 1995;Feigenspan et al., 2001;Massey and Mills, 1999). Although these markers failed to label Cx36-containing AII amacrine cells in mouse retina, calretinin was found to be adequate for labeling of other types of amacrine cell somata in the INL and ganglion cell layer, as well as for labeling the dendritic arborizations of these cells in three distinct bands of roughly equal thickness in the outer OFF-sublamina of the IPL (Haverkamp and Wässle, 2000). Among these calretinin bands, Cx36/ZO-1//ZO-2/ZONAB puncta were distributed between the two outer calretinin bands and intermingled with the outer band. Previous studies of Cx36 in the outer region of the IPL excluded association of Cx36-puncta with appendages of AII amacrine cells distributed in this region, even though dendrites of these cells are heavily coupled by Cx36 in the inner part of IPL (Feigenspan et al., 2001). Likely candidates for the origin of these Cx36-puncta are OFF-alpha-ganglion cells, some of which have dendritic terminal fields distributed in the outer IPL (Sun et al., 2002;Famiglietti and Kolb, 1976;Nelson et al., 1978), specifically in the region of the outer two calretinin-positive bands. These alpha-ganglion cells were reported to be gap junctionally coupled with each other via Cx36, but they also are junctionally coupled with wide-field amacrine cells that lack Cx36 expression (Vaney, 1991,1994;Penn et al., 1994;Jacoby et al., 1996;Hu and Bloomfield, 2003;Schubert et al., 2005). Thus, it was suggested that Cx36 in alpha-ganglion cells form junctions with an as yet unidentified Cx expressed in wide-field amacrine cells (Schubert et al., 2005).

The apparent expression of an unidentified connexin in wide-field amacrine cells provides a plausible explanation for the persistence of ZO-1/ZO-2/ZONAB co-localized puncta in the outer region of the IPL in Cx36 KO mice. Thus, these puncta may represent ZO-1/ZO-2/ZONAB association with hemiplaques containing an unknown connexin expressed in wide-field amacrine cells, which ordinarily couple with hemiplaques of Cx36 in alpha-ganglion cells or, alternatively, association with an unidentified connexin that forms gap junctions between wide-field amacrine cells (Kolb and Nelson, 1984, 1985). Based on FRIL observations of the presence of ZO-1 at PSDs, however, we cannot rule out the possibility that ZO-1/ZO-2/ZONAB may be associated with clusters of neurotransmitter receptor and/or presynaptic active zones. Investigation of these possibilities will require EM analyses to establish the presence of ultrastructurally-identified gap junctions in the outer part of the IPL in Cx36 KO mice, and demonstration of the association of ZO-1, ZO-2 and ZONAB with these hypothetical junctions.

Acknowledgments

This work was supported by grants from the Canadian Institutes of Health Research to J.I.N., by NIH grants NS31027, NS44010, and NS 44195 to J.E.R., and a Manitoba Health Research Council Studentship to C.O. We thank B. McLean, N. Nolette and J. A. Sampson for excellent technical assistance, and Dr. D. Paul (Harvard University) for providing a breeding pair of $Cx36^{\pm}$ mice.

Abbreviations

ATCC, American Type Culture Collection
Cx, connexin
Cx36, connexin36
FRIL, freezer-fracture replica immunogold labeling
IMP, intramembrane particles
INL, inner nuclear layer
IP, immunoprecipitation
IPL, inner plexiform layer

KO, knockout
MAGUK, membrane-associated, guanylate kinase-lik
OLM, outer limiting membran
OPL, outer plexiform laye
PDZ domain, postsynaptic protein PSD95/*Drosophila* junction protein Disc-large/zonula occludens-
PSDs, post-synaptic densitie
RIS, rod inner segmen
ROS, rod outer segmen
SDS, sodium dodecylsulfat
SDS-PAGE, SDS-polyacrylamide gel electrophoresi
TBSTr, 50 mM Tris–HCl, pH 7.4, containing 256 mM sodium chloride and 0.3% Triton X-100
TBSTw, 10 mM Tris–HCl, pH 8.0, 150 mM NaCl, 0.2% Tween-20
WT, wild-type
ZONAB, zonula occludens-1-associated nucleic acid-binding protein
ZO-1, zonula occludens-1
ZO-2, zonula occludens-2

REFERENCES

Balda MS, Matter K. The tight junction protein ZO-1 and an interacting transcription factor regulate ErbB-2 expression. EMBO J 2000;19:2024–2033. [PubMed: 10790369]

Balda MS, Matter K. Epithelial cell adhesion and the regulation of gene expression. Trends Cell Biol 2003;13:310–318. [PubMed: 12791297]

Balda MS, Garrett MD, Matter K. The ZO-1-associated Y-box factor ZONAB regulates epithelial cell proliferation and cell density. J Cell Biol 2003;160:423–432. [PubMed: 12566432]

Becker D, Bonness V, Mobbs P. Cell coupling in the retina: patterns and purpose. Cell Biol Int 1998;22:781–792. [PubMed: 10873291]

Bennett MVL. Gap junctions as electrical synapses. J Neurocytol 1997;26:349–366. [PubMed: 9278865]

Bennett MVL, Zukin RS. Electrical coupling and neuronal synchronization in the mammalian brain. Neuron 2004;41:495–511. [PubMed: 14980200]

Bermingham-McDonogh O, McCabe KL, Reh TA. Effects of GGF/neuregulins on neuronal survival and neurite outgrowth correlate with erbB2/neu expression in developing rat retina. Development 1996;122:1427–1438. [PubMed: 8625831]

Casalini P, Iorio MV, Galmozzi E, Menard S. Role of HER receptors family in development and differentiation. J Cell Physiol 2004;200:343–350. [PubMed: 15254961]

Casini G, Rickman DW, Brecha NC. AII amacrine cell population in the rabbit retina: identification by parvalbumin immunoreactivity. J Comp Neurol 1995;35:132–142. [PubMed: 7629307]

Collins JR, Rizzolo LJ. Protein-binding domains of the tight junction protein, ZO-2, are highly conserved between avian and mammalian species. Biochem Biophys Res Commun 1998;252:617–622. [PubMed: 9837755]

Connors BW, Long MA. Electrical synapses in the mammalian brain. Annu Rev Neurosci 2004;27:393–418. [PubMed: 15217338]

Davies HG, Giorgini F, Fajardo MA, Braun RE. A sequence-specific RNA binding complex expressed in murine germ cells contains MSY2 and MSY4. Dev Biol 2000;221:87–100. [PubMed: 10772793]

Deans MR, Gibson JR, Sellitto C, Connors BW, Paul DL. Synchronous activity of inhibitory networks in neocortex requires electrical synapses containing connexin36. Neuron 2001;31:477–485. [PubMed: 11516403]

Deans MR, Volgyi B, Goodenough DA, Bloomfield SA, Paul DL. Connexin36 is essential for transmission of rod-mediated visual signals in the mammalian retina. Neuron 2002;36:703–712. [PubMed: 12441058]

Famiglietti EV Jr, Kolb H. A bistratified amacrine cell and synaptic circuitry in the inner plexiform layer of the retina. Brain Res 1975;84:293–300. [PubMed: 1111833]

Famiglietti EV Jr, Kolb H. Structural basis for ON- and OFF-center responses in retinal ganglion cells. Science 1976;194:193–195. [PubMed: 959847]

Feigenspan A, Teubner B, Willecke K, Weiler R. Expression of neuronal connexin36 in AII amacrine cells of the mammalian retina. J Neurosci 2001;21:230–239. [PubMed: 11150340]

Feigenspan A, Janssen-Bienhold U, Hormuzdi S, Monyer H, Degen J, Söhl G, Willecke K, Ammermuller J, Weiler R. Expression of connexin36 in cone pedicles and OFF-cone bipolar cells of the mouse retina. J Neurosci 2004;24:3325–3334. [PubMed: 15056712]

Fujimoto K. Freeze-fracture replica electron microscopy combined with SDS digestion for cytochemical labelling of integral membrane proteins. Application to the immunogold labelling of intercellular junctional complexes. J Cell Sci 1995;108:3443–3449. [PubMed: 8586656]

Gabriel R, Straznicky C. Immunocytochemical localization of parvalbumin- and neurofilament triplet protein-immunoreactivity in the cat retina: colocalization in a subpopulation of AII amacrine cells. Brain Res 1992;595:133–136. [PubMed: 1467949]

Giepmans BN, Moolenaar WH. The gap junction protein connexin43 interacts with the second PDZ domain of the zonula occludens-1 protein. Curr Biol 1998;8:931–934. [PubMed: 9707407]

Giepmans BN. Gap junctions and connexin-interacting proteins. Cardiovasc Res 2004;62:233–245. [PubMed: 15094344]

Giorgini F, Davies HG, Braun RE. MSY2 and MSY4 bind a conserved sequence in the 3′ untranslated region of protamine 1 mRNA in vitro and in vivo. Mol Cell Biol 2001;21:7010–7019. [PubMed: 11564883]

Giorgini F, Davies HG, Braun RE. Translational repression by MSY4 inhibits spermatid differentiation in mice. Development 2002;129:3669–3679. [PubMed: 12117816]

González-Mariscal L, Betanzos A, Avila-Flores A. MAGUK proteins: structure and role in the tight junction. Semin Cell Dev Biol 2000;11:315–324. [PubMed: 10966866]

González-Mariscal L, Betanzos A, Nava P, Jaramillo BE. Tight junction proteins. Prog Biophys Mol Biol 2003;81:1–44. [PubMed: 12475568]

Goodenough DA, Goliger JA, Paul DL. Connexins, connexons, and intercellular communication. Annu Rev Biochem 1996;65:475–502. [PubMed: 8811187]

Güldenagel M, Söhl G, Plum A, Traub O, Teubner B, Weiler R, Willecke K. Expression patterns of connexin genes in mouse retina. J Comp Neurol 2000;425:193–201. [PubMed: 10954839]

Güldenagel M, Ammermuller J, Feigenspan A, Teubner B, Degen J, Söhl G, Willecke K, Weiler R. Visual transmission deficits in mice with targeted disruption of the gap junction gene connexin36. J Neurosci 2001;21:6036–6044. [PubMed: 11487627]

Harris KM, Landis DMD. Membrane structure at synaptic junctions in area CA1 of the rat hippocampus. Neuroscience 1986;19:857–872. [PubMed: 3796819]

Haverkamp S, Wässle H. Immunocytochemical analysis of the mouse retina. J Comp Neurol 2000;424:1–23. [PubMed: 10888735]

He S, Weiler R, Vaney DI. Endogenous dopaminergic regulation of horizontal cell coupling in the mammalian retina. J Comp Neurol 2000;418:33–40. [PubMed: 10701754]

Hervé JC, Bourmeyster N, Sarrouilhe D. Diversity in protein-protein interactions of connexins: emerging roles. Biochim Biophys Acta 2004;1662:22–41. [PubMed: 15033577]

Hidaka S, Kato T, Miyachi E. Expression of gap junction connexin36 in adult rat retinal ganglion cells. J Integr Neurosci 2004;1:3–22. [PubMed: 15011262]

Holbro T, Hynes NE. ErbB receptors: directing key signaling networks throughout life. Annu Rev Pharmacol Toxicol 2004;44:195–217. [PubMed: 14744244]

Hombach S, Janssen-Bienhold U, Söhl G, Schubert T, Bussow H, Ott T, Weiler R, Willecke K. Functional expression of connexin57 in horizontal cells of the mouse retina. Eur J Neurosci 2004;19:2633–2640. [PubMed: 15147297]

Hu EH, Bloomfield SA. Gap junctional coupling underlies the short-latency spike synchrony of retinal alpha ganglion cells. J Neurosci 2003;23:6768–6777. [PubMed: 12890770]

Huang H, Li H, He SG. Identification of connexin 50 and 57 mRNA in A-type horizontal cells of the rabbit retina. Cell Res 2005;15:207–211. [PubMed: 15780184]

Inoko A, Itoh M, Tamura A, Matsuda M, Furuse M, Tsukita S. Expression and distribution of ZO-3, a tight junction MAGUK protein, in mouse tissues. Genes Cells 2003;8:837–845. [PubMed: 14622136]

Itoh M, Morita K, Tsukita S. Characterization of ZO-2 as a MAGUK family member associated with tight as well as adherens junctions with a binding affinity to occludin and alpha-catenin. J Biol Chem 1999a;274:5981–5986. [PubMed: 10026224]

Itoh M, Furuse M, Morita K, Kubota K, Saitou M, Tsukita S. Direct binding of three tight junction-associated MAGUKs, ZO-1, ZO-2 and ZO-3, with the COOH termini of claudins. J Cell Biol 1999b; 147:1351–1363. [PubMed: 10601346]

Jacoby R, Stafford D, Kouyama N, Marshak D. Synaptic inputs to ON parasol ganglion cells in the primate retina. J Neurosci 1996;16:8041–8056. [PubMed: 8987830]

Janssen-Bienhold U, Schultz K, Hoppenstedt W, Weiler R. Molecular diversity of gap junctions between horizontal cells. Prog Brain Res 2001;131:93–107. [PubMed: 11420985]

Jeon MH, Jeon CJ. Immunocytochemical localization of calretinin containing neurons in retina from rabbit, cat, and dog. Neurosci Res 1998;32:75–84. [PubMed: 9831254]

Kausalya PJ, Reichert M, Hunziker W. Conneixn45 directly binds to ZO-1 and localizes to the tight junction region in epithelial MDCK cells. FEBS Lett 2001;505:92–96. [PubMed: 11557048]

Kojima T, Kokai Y, Chiba H, Yamamoto M, Mochizuki Y, Sawada N. Cx32 but not Cx26 is associated with tight junctions in primary cultures of rat hepatocytes. Exp Cell Res 2001;263:193–201. [PubMed: 11161718]

Kolb H, Nelson R. Neural architecture of the cat retina. Prog Ret Res 1984;3:21–60.

Kolb, H.; Nelson, R. Functional circuitry of amacrine cells in the cat retina. In: Gallego, A.; Gouras, P., editors. Neurocircuitry of the retina: a Cajal memorial. Elsevier Press; New York: 1985. p. 215-232.

Kumar NM, Gilula NB. The gap junction communication channel. Cell 1996;84:381–388. [PubMed: 8608591]

Laing JG, Manley-Markowski RN, Koval M, Civitelli R, Steinberg TH. Connexin45 interacts with zonula occludens-1 and conneixn43 in osteoblastic cells. J Biol Chem 2001;276:23051–23055. [PubMed: 11313345]

LaVail MM. Survival of some photoreceptor cells in albino rats following long-term exposure to continuous light. Invest Opthalmol 1976;15:64–70.

Lee EJ, Han JW, Kim HJ, Kim IB, Lee MY, Oh SJ, Chung JW, Chun MH. The immunocytochemical localization of connexin 36 at rod and cone gap junctions in the guinea pig retina. Eur J Neurosci 2003;18:2925–2934. [PubMed: 14656288]

Li L, Backer J, Wong ASK, Schwanke EL, Stewart BG, Pasdar M. Bcl-2 expression decreases cadherin-mediated cell-cell adhesion. J Cell Sci 2003;116:3687–3700. [PubMed: 12890751]

Li X, Olson C, Lu S, Kamasawa N, Yasumura T, Rash JE, Nagy JI. Neuronal connexin36 association with zonula occludens-1 protein (ZO-1) in mouse brain and interaction with the first PDZ domain of ZO-1. Eur J Neurosci 2004a;19:2132–2146. [PubMed: 15090040]

Li X, Olson C, Lu S, Nagy JI. Association of connexin36 with zonula occludens-1 in HeLa cells, βTC-3 cells, pancreas and adrenal gland. Histochem Cell Biol 2004b;122:485–498. [PubMed: 15558297]

Li X, Ionescu AV, Lynn BD, Lu S, Kamasawa N, Morita M, Davidson KG, Yasumura T, Rash JE, Nagy JI. Connexin47, connexin29 and connexin32 co-expression in oligodendrocytes and Cx47 association with zonula occludens-1 (ZO-1) in mouse brain. Neuroscience 2004c;126:611–630. [PubMed: 15183511]

Lindqvist N, Vidal-Sanz M, Hallbook F. Single cell RT-PCR analysis of tyrosine kinase receptor expression in adult rat retinal ganglion cells isolated by retinal sandwiching. Brain Res Protoc 2002;10:75–83.

Marmor MD, Skaria KB, Yarden Y. Signal transduction and oncogenesis by ErbB/HER receptors. Int J Radiat Oncol Biol Phys 2004;58:903–913. [PubMed: 14967450]

Massey SC, Mills SL. Antibody to calretinin stains AII amacrine cells in the rabbit retina: double-label and confocal analyses. J Comp Neurol 1999;411:3–18. [PubMed: 10404104]

Massey SC, O'Brien JJ, Trexler EB, Li W, Keung JW, Mills S, O'Brien J. Multiple neuronal connexins in the mammalian retina. Cell Commun Adhes 2003;10:425–430. [PubMed: 14681052]

Mastrangelo MA, Kleene KC. Developmental expression of Y-box protein 1 mRNA and alternatively spliced Y-box protein 3 mRNAs in spermatogenic cells in mice. Mol Hum Reprod 2000;6:779–788. [PubMed: 10956549]

Mills SL, O'Brien JJ, Li W, O'Brien J, Massey SC. Rod pathways in the mammalian retina use connexin 36. J Comp Neurol 2001;436:336–350. [PubMed: 11438934]

Nelson R, Famiglietti EV Jr, Kolb H. Intracellular staining reveals different levels of stratification for on- and off-center ganglion cells in cat retina. J Neurophysiol 1978;41:472–483. [PubMed: 650277]

Nielsen PA, Beahm DL, Giepmans BN, Baruch A, Hall JE, Kumar NM. Molecular cloning, functional expression, and tissue distribution of a novel human gap junction-forming protein, connexin31.9. Interaction with zonula occludens protein-1. J Biol Chem 2002;277:38272–38283. [PubMed: 12154091]

Nielsen PA, Baruch A, Shestopalov VI, Giepmans BN, Benedetti EI, Kumar NM. Lens connexins Cx46 and Cx50 interact with zonula occludens protein-1 (ZO-1). Mol Biol Cell 2003;14:2470–2481. [PubMed: 12808044]

Paffenholz R, Kuhn C, Grund C, Stehr S, Franke WW. The arm-repeat protein NPRAP (neurojungin) is a constituent of the plaques of the outer limiting zone in the retina, defined a novel type of adhering junction. Exp Cell Res 1999;250:452–464. [PubMed: 10413599]

Penes M, Li X, Nagy JI. Expression of zonula occludens-1 (ZO-1) and the transcription factor ZO-1-associated nucleic acid-binding protein (ZONAB/MsY3) in glial cells and co-localization at oligodendrocyte and astrocyte gap junctions in mouse brain. Eur J Neurosci 2005;22:404–418. [PubMed: 16045494]

Penn AA, Wong RO, Shatz CJ. Neuronal coupling in the developing mammalian retina. J Neurosci 1994;14:309–324.

Pereda A, O'Brien J, Nagy JI, Bukauskas F, Davidson KGV, Kamasawa N, Yasumura T, Rash JE. Connexin35 mediates electrical transmission at mixed synapses on Mauthner cells. J Neurosci 2003a; 23:7489–7503. [PubMed: 12930787]

Pereda A, O'Brien J, Nagy JI, Smith M, Bukauskas F, Davidson KGV, Kamasawa N, Yasumura T, Rash JE. Short-range functional interaction between connexin35 and neighboring chemical synapses. Cell Commun Adhes 2003b;10:419–423. [PubMed: 14681051]

Pereda A, Rash JE, Nagy JI, Bennett MVL. Dynamics of electrical transmission at club endings on the Mauthner cells. Brain Res Rev 2004;47:227–244. [PubMed: 15572174]

Rash JE, Pereda A, Kamasawa N, Furman CS, Yasumura T, Davidson KGV, Dudek FE, Olson C, Li X, Nagy JI. High-resolution proteomic mapping in the vertebrate central nervous system: Close proximity of connexin35 to NMDA glutamate receptor clusters and co-localization of connexin36 with immunoreactivity for zonula occludens protein-1 (ZO-1). J Neurocytol 2004;33:131–151. [PubMed: 15173637]

Rash JE, Yasumura T. Direct immunogold labelling of connexins and aquaporin4 in freeze-fracture replicas of liver, brain and spinal cord: factors limiting quantitative analysis. Cell Tissue Res 1999;296:307–321. [PubMed: 10382274]

Rash JE, Staines WA, Yasumura T, Patel D, Furman CS, Stelmack GL, Nagy JI. Immunogold evidence that neuronal gap junctions in adult rat brain and spinal cord contain connexin36 but not connexin32 or connexin43. Proc Natl Acad Sci U S A 2000;97:7573–7578. [PubMed: 10861019]

Scadding JW. Development of ongoing activity, mechanosensitivity, and adrenaline sensitivity in severed peripheral nerve axons. Exp Neurol 1981;73:345–364. [PubMed: 7262242]

Schubert T, Degen J, Willecke K, Hormuzdi SG, Monyer H, Weiler R. Connexin36 mediates gap junctional coupling of alpha-ganglion cells in mouse retina. J Comp Neurol 2005;485:191–201. [PubMed: 15791644]

Sharpe LT, Stockman A. Rod pathways: the importance of seeing nothing. Trends Neurosci 1999;22:497–504. [PubMed: 10529817]

Singh D, Lampe PD. Identification of connexin-43 interacting proteins. Cell Commun Adhes 2003;10:215–220. [PubMed: 14681019]

Singh D, Solan JL, Taffet SM, Javier R, Lampe PD. Connexin43 interacts with zona occludens-1 and -2 proteins in a cell cycle stage-specific manner. J Biol Chem 2005;280:30416–30421. [PubMed: 15980428]

Söhl G, Güldenagel M, Traub O, Willecke K. Connexin expression in the retina. Res Brain Res Rev 2000;32:138–145.

Strettoi E, Raviola E, Dacheux RF. Synaptic connections of the narrow-field, bistratified rod amacrine cell (AII) in the rabbit retina. J Comp Neurol 1992;325:152–168. [PubMed: 1460111]

Sun W, Li N, He S. Large-scale morphological survey of mouse retinal ganglion cells. J Comp Neurol 2002;451:115–126. [PubMed: 12209831]

Toyofuku T, Yabuki M, Otsu K, Kuzuya T, Hori M, Tada M. Direct association of the gap junction protein connexin-43 with ZO-1 in cardiac myocytes. J Biol Chem 1998;273:12725–12731. [PubMed: 9582296]

Tserentsoodol N, Shin B-C, Suzuki T, Takata K. Colocalization of tight junction proteins, occludin and ZO-1, and glucose transporter GLUT1 in cells of the blood-ocular barrier in the mouse eye. Histochem Cell Biol 1998;110:543–551. [PubMed: 9860252]

Vaney DI. Many diverse types of retinal neurons show tracer coupling when injected with biocytin or neurobiotin. Neurosci Lett 1991;125:187–190. [PubMed: 1715532]

Vaney DI. Patterns of neuronal coupling in the retina. Prog Ret Eye Res 1994;13:301–355.

Vaney DI. Neuronal coupling in the central nervous system: lessons from the retina. Novartis Found Symp 1999;219:113–125. [PubMed: 10207901]

Wässle H, Grunert U, Rohrenbeck J. Immunocytochemical staining of AII-amacrine cells in the rat retina with antibodies against parvalbumin. J Comp Neurol 1993;332:407–420. [PubMed: 8349840]

Wässle H, Grunert U, Chun MH, Boycott BB. The rod pathway of the macaque monkey retina: identification of AII-amacrine cells with antibodies against calretinin. J Comp Neurol 1995;361:537–551. [PubMed: 8550898]

Weiler R, He S, Vaney DI. Retinoic acid modulates gap junctional permeability between horizontal cells of the mammalian retina. Eur J Neurosci 1999;11:3346–3350. [PubMed: 10510200]

Weiler R, Pottek M, He S, Vaney DI. Modulation of coupling between retinal horizontal cells by retinoic acid and endogenous dopamine. Res Brain Res Rev 2000;32:121–129.

Willecke K, Eiberger J, Degen J, Eckardt D, Romualdi A, Güldenagel M, Deutsch U, Söhl G. Structural and functional diversity of connexin genes in the mouse and human genome. Biol Chem 2002;383:725–737. [PubMed: 12108537]

Williams CD, Rizzolo LJ. Remodeling of junctional complexes during the development of the outer blood-retinal barrier. Anat Rec 1997;249:380–388. [PubMed: 9372172]

Williams RW, Strom RC, Goldowitz D. Natural variation in neuron number in mice is linked to a major quantitative trait locus on Chr 11. J Neurosci 1998;18:138–146. [PubMed: 9412494]

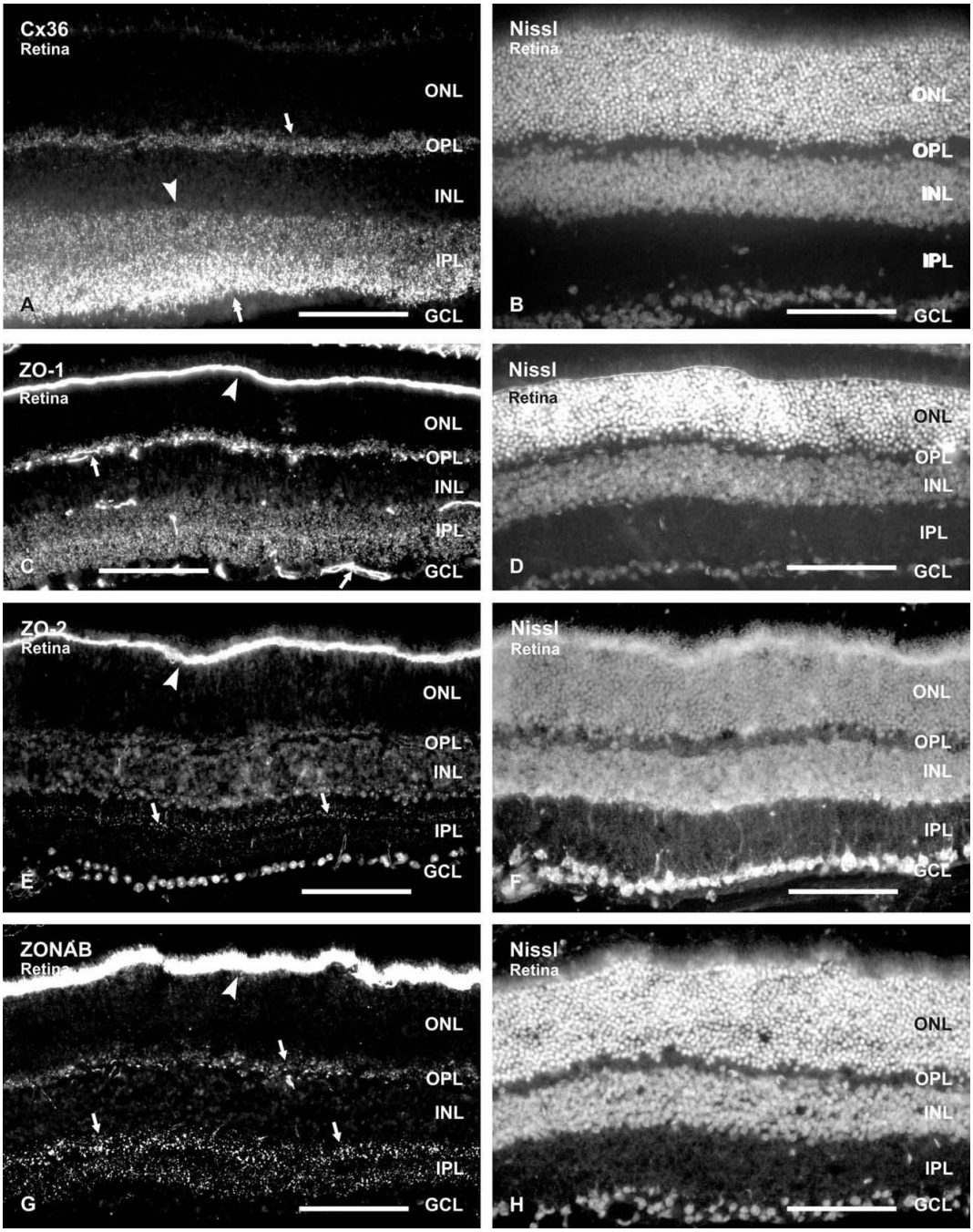

Fig. 1.

Relative densities of Cx36, ZO-1, ZO-2 and ZONAB in adult mouse retina. (A–H) Each pair of images (A, B), (C, D), (E, F) (G, H) shows fields of vertical retinal sections labeled by immunofluorescence for the proteins indicated (A, C, E, G) and the same fields counterstained with fluorescence Nissl Neurotrace (B, D, F, H, respectively). Labeling of each protein appears punctate, and ZO-1 is also evident along blood vessels (C, arrows). Cx36 is dense in the inner half of IPL (A, double arrow), and less dense in the outer half of IPL (A, arrowhead) and the OPL (A, arrow). ZO-1 is dense to moderate in both IPL and OPL (C). ZO-2 is sparse throughout the IPL, and is seen as a band of puncta in the outer IPL (E, arrows). ZONAB is moderate in

both the IPL and OPL (G, arrows). The OLM is very densely labeled for ZO-1, ZO-2 and ZONAB (C, E, G, arrowheads). Scale bars=100 μm.

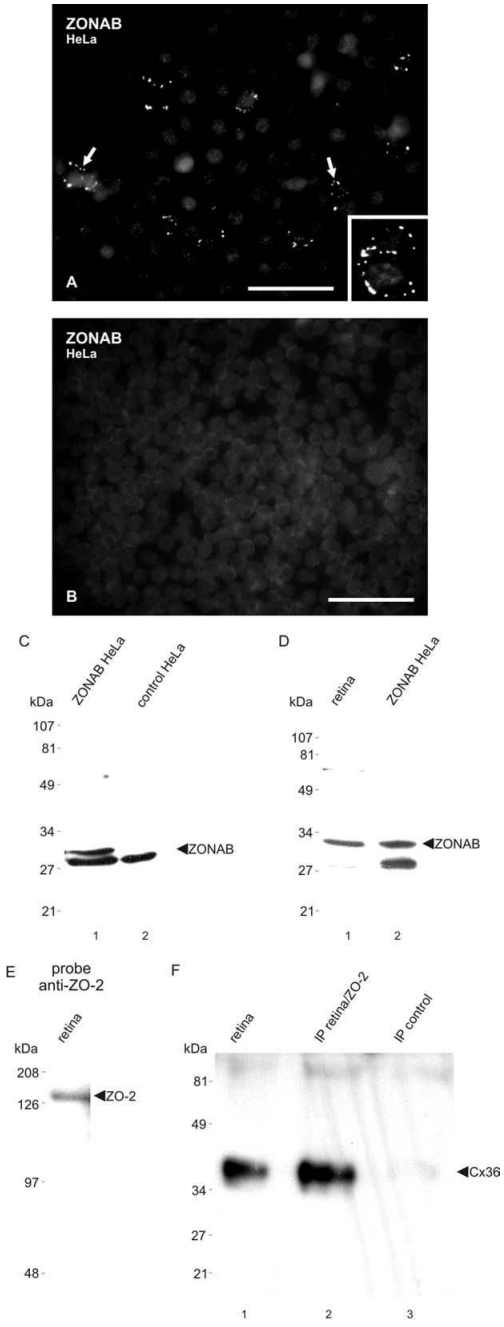

Fig. 2.

Characterization of anti-ZONAB and anti-ZO-2 antibodies. (A, B) Immunofluorescence detection of ZONAB in HeLa cells transiently transfected with ZONAB cDNA (A) and absence of labeling in control empty vector-transfected HeLa cells (B). Labeling is seen as ZONAB-positive puncta around the periphery of individual cells (A, arrows; magnified in inset). (C) Immunoblot showing detection of ZONAB in HeLa cells transiently transfected with ZONAB (lane 1), and absence of a corresponding band in control empty vector-transfected HeLa cells (lane 2). ZONAB is seen migrating at approximately 31 kDa. A protein migrating at about 28 kDa is detected by anti-ZONAB in transfected and control HeLa cells (lane 3), and is of uncertain identity. (D) Immunoblot showing detection of ZONAB in mouse retina, with

migration profile corresponding to that in ZONAB-transfected HeLa cells. (E) Immunoblot of mouse retina probed with anti-ZO-2 Ab71-1400, showing ZO-2 migrating at 160 kDa. (F) Immunoblot showing detection of Cx36 after IP of ZO-2 from retinal homogenate (lane 2), with a positive control lane showing detection of Cx36 in homogenate of retina (lane 1), and absence of Cx36 detection after omission of anti-ZO-2 during the IP procedure (lane 3). Scale bars=50 μm A; B, 100 μm.

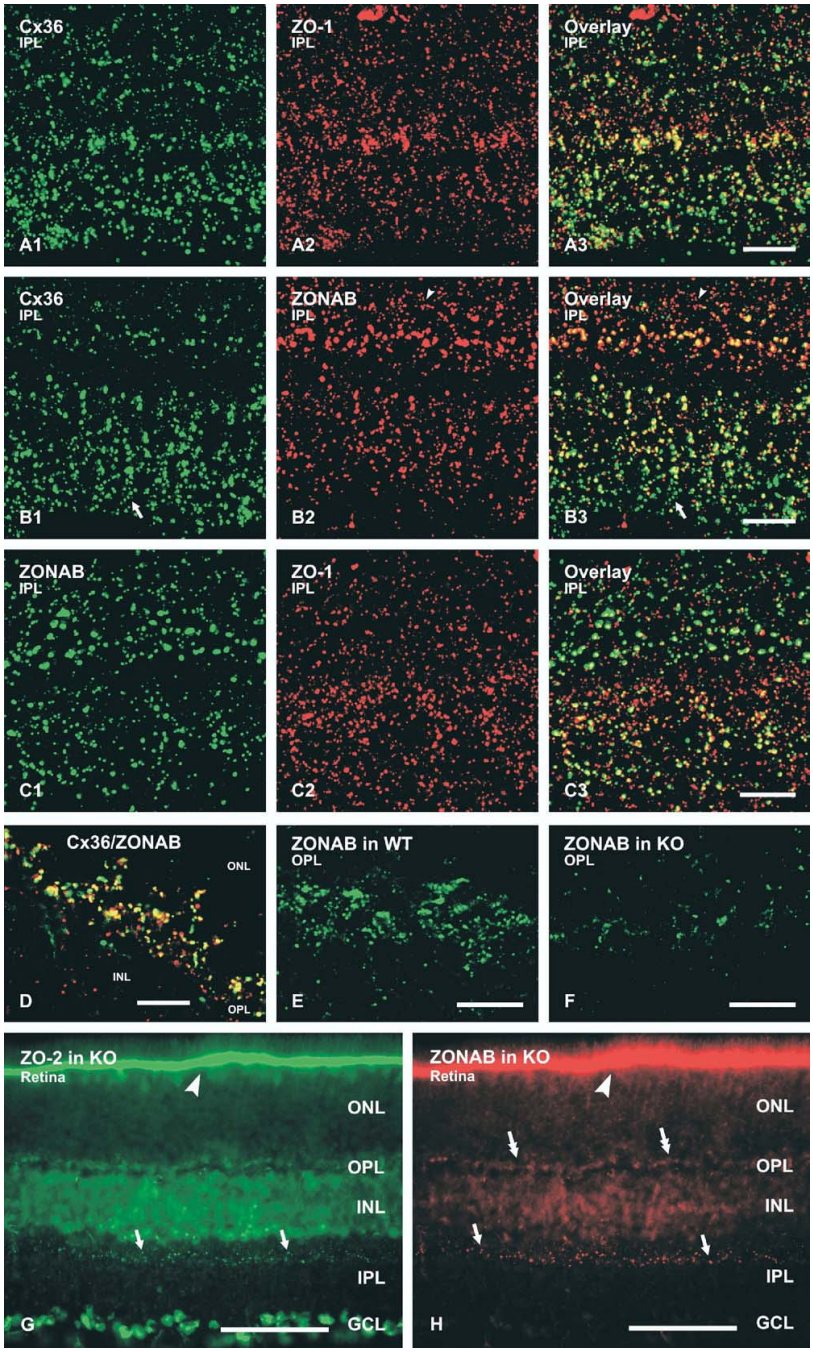

Fig. 3.

(A–F) Laser scanning confocal double immunofluorescence of Cx36, ZO-1 and ZONAB in vertical sections of adult mouse retina. Images in A–C show the entirety of IPL from inner (bottom) to outer (top) edge, and represent Z-stacks of five scans. Overlap of green and red labeling is seen as yellow in overlay images. (A) Images of the same field showing that most Cx36-positive puncta are positive for ZO-1, but not all ZO-1-puncta are positive for Cx36. (B) Images of the same field showing that many Cx36-puncta in the IPL are positive for ZONAB, except those in the extreme inner region that lack ZONAB (B1, B3, arrow). The extreme outer region contains many ZONAB-puncta (B2, arrowhead) lacking Cx36 (B3, arrowhead). (C) Images of the same field showing that many ZONAB-puncta are positive for ZO-1, but not all

ZO-1 puncta are positive for ZONAB. (D) Single confocal scan overlay showing that most Cx36-positive puncta (green) in the OPL are positive for ZONAB (red). (E, F) Single confocal scans showing punctate labeling of ZONAB in the OPL of WT retina (E), and a large reduction of ZONAB-positive puncta in the OPL of retina from Cx36 KO mice. (G, H) Low magnifications immunofluorescence images showing ZO-2 (G) and ZONAB (H) in retina of Cx36 KO mice. Labeling for both proteins persists in the outer region of the IPL (arrows) and at the OLM (arrowheads), but is reduced in the inner part of the IPL. Labeling for ZONAB is also reduced in the OPL (double arrowheads). Scale bars=10 μm A–F; G, H, 100 μm.

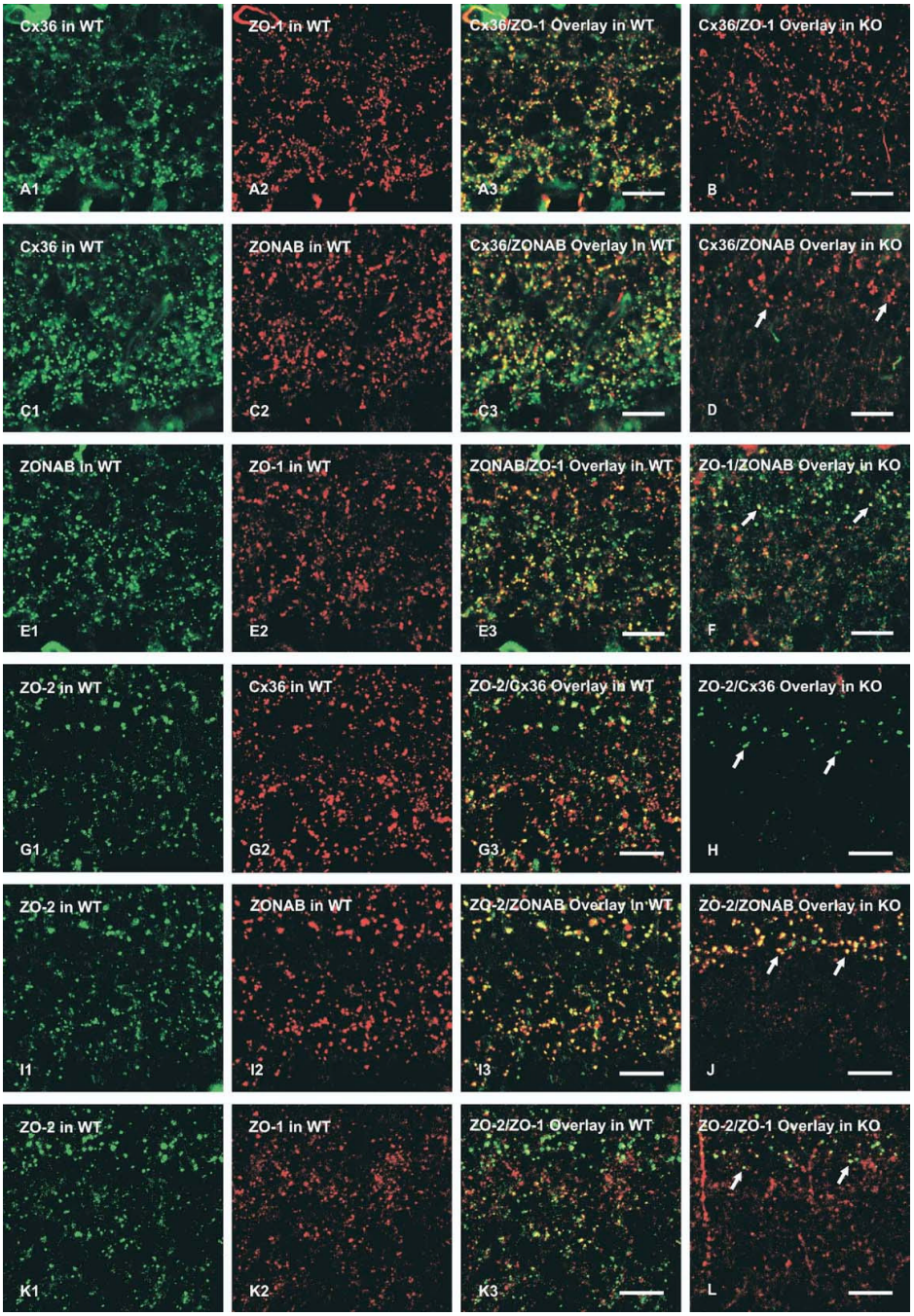

Fig. 4.

Immunofluorescence labeling of Cx36, ZO-1, ZO-2 and ZONAB in the IPL of retina from adult WT and Cx36 KO C57BL6/129SvEv mice. Images show the entirety of the IPL in vertical sections, and represent single confocal scans (A–F) or Z-stacks of five scans (G–L). The first three panels in each horizontal row of images show the same field of the IPL double-labeled for the proteins indicated in WT mice, and the fourth panel in each row shows labeling of the same proteins with the same fluorochrome colors in image overlays of IPL from retina of Cx36 KO mice. Overlap of green and red is seen as yellow. (A, B) Co-localization of Cx36 and ZO-1 is seen in the IPL of WT mice (A), while Cx36 is absent (B) and ZO-1 is slightly reduced (B) in the IPL of Cx36 KO mice. (C, D) Co-localization of Cx36 and ZONAB is seen in the IPL

of WT mice (C), and the absence of Cx36 in Cx36 KO mice (D) is accompanied by a reduction of ZONAB in all but the outer one-third margin of the IPL (D, arrows). (E, F) Co-localization of ZO-1/ZONAB is seen in the IPL of WT mice (E), and persists in the outer third of the IPL in Cx36 KO mice (F, arrows). (G, H) Nearly all ZO-2-puncta are seen co-localized with Cx36, but not all Cx36-puncta are positive for ZO-2 in the IPL of WT mice (G), and absence of Cx36 in Cx36 KO mice is accompanied by a large reduction of ZO-2 in all but the outer margin of the IPL (H, arrows). (I, J) Most ZO-2-puncta are seen labeled for ZONAB in the IPL of WT mice (I), and ZO-2 and ZONAB persisting in the outer margin of the IPL in Cx36 KO mice remain co-localized (J, arrows). (K, L) ZO-2 is co-localized with ZO-1 in the IPL of WT mice (K), and co-localization persists in the outer margin of the IPL in Cx36 KO mice (L, arrows). Scale bars=10 μm.

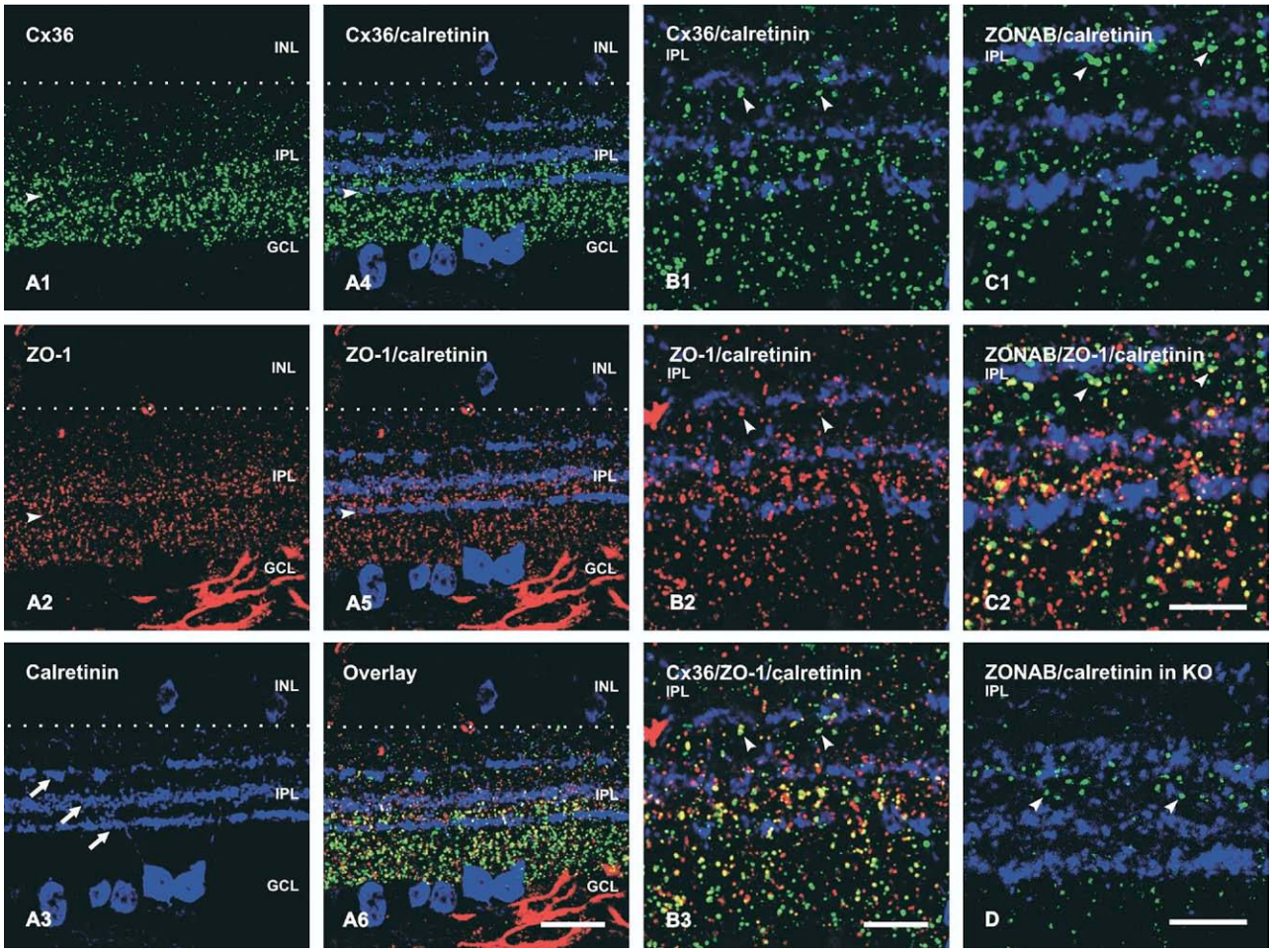

Fig. 5.

Triple immunofluorescence labeling showing the distribution of Cx36, ZO-1 and ZONAB in relation to the sublaminar arrangement of calretinin-positive processes in the IPL of adult mouse retina. (A) Low magnifications of the same field show Cx36 (A1), ZO-1 (A2) and calretinin (A3) in relation to the retinal layers, and Cx36/calretinin in overlay (A4), ZO-1/calretinin in overlay (A5) and Cx36/ZO-1/calretinin in overlay (A6). The processes of calretinin-positive amacrine cells form three parallel bands (A3, arrows) in the outer part of the IPL, with the outer band located near the IPL/INL border (dotted line). Cx36 and ZO-1 are relatively sparse along the inner band (arrowheads), and are more concentrated between the inner two bands. (B) Higher magnifications of the same field showing Cx36 (green) with calretinin (blue) (B1), ZO-1 (red) with calretinin (blue) (B2), and Cx36/ZO-1/calretinin in overlay (B3). Cx36-puncta co-localized with ZO-1 are seen throughout the IPL, including the region between the outer calretinin-positive bands (arrowheads). (C) Higher magnifications of the same field showing ZONAB (green) with calretinin (blue) (C1), and ZONAB (green), ZO-1 (red) with calretinin (blue) (C2) in overlay. ZONAB-puncta (C1, arrowheads) co-localized with ZO-1 (C2, arrowheads) are seen between the outer calretinin-positive bands. (D) Double labeling of ZONAB and calretinin in retina of Cx36 KO mice, showing the persistence of intensely labeled ZONAB-positive puncta between the outer two calretinin-positive bands (arrowheads). Scale bars=20 μm A1–A6; B–D, 10 μm.

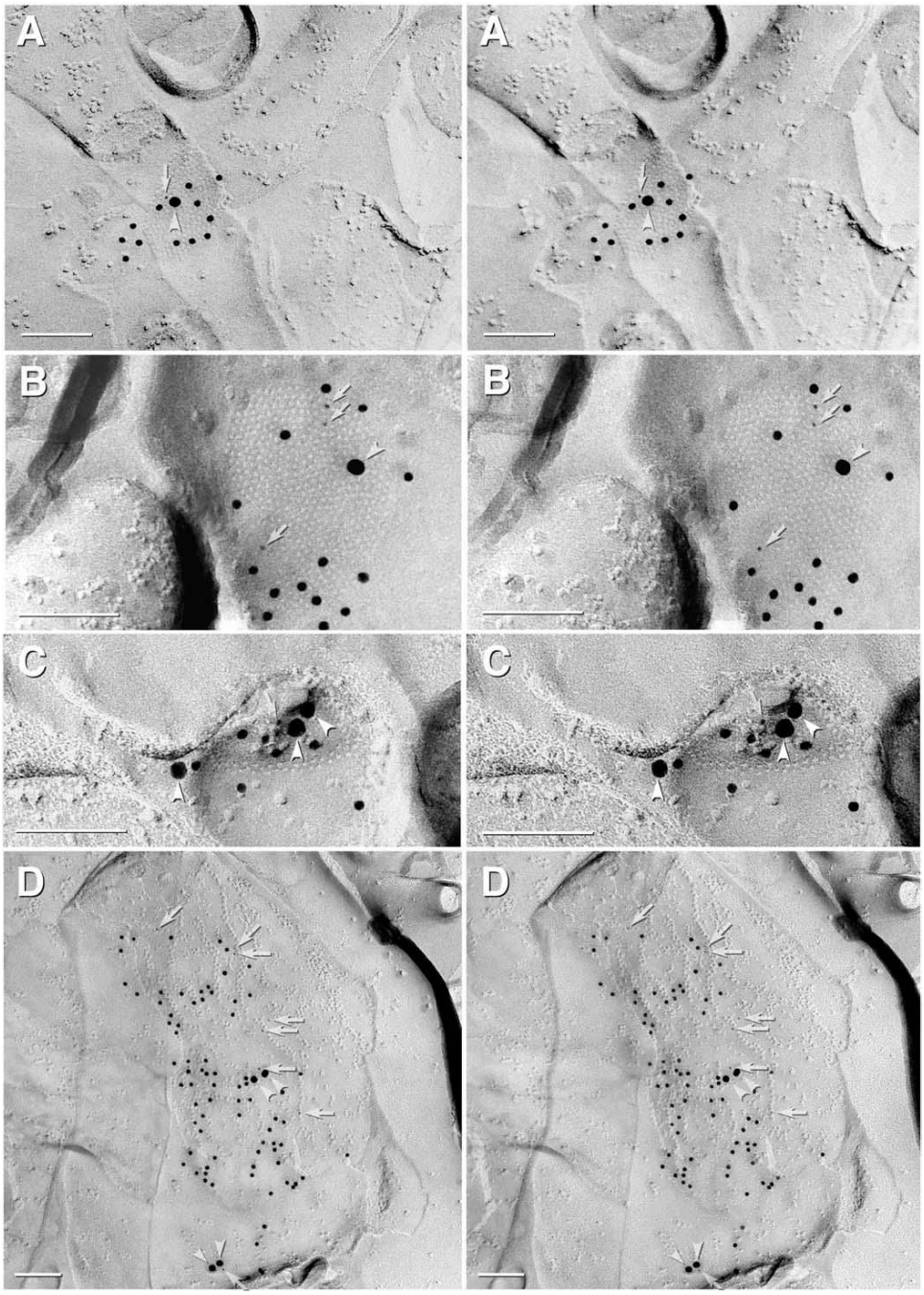

Fig. 6.

FRIL of gap junctions in rat retina after double labeling for Cx36 and ZO-2. (A) Two very small dendrites in the IPL are linked by a small plaque-type gap junction that is double labeled for Cx36 with 12 12-nm gold beads, and for ZO-2 with one 6-nm gold bead (arrow) and one 18-nm gold bead (arrowhead). (B) A large regular plaque-type gap junction in the inner IPL labeled for Cx36 with 14 12-nm gold beads, and for ZO-2 with three 6-nm gold beads (arrows), and one 18-nm gold bead (arrowhead). (C) Small reticular-type gap junction labeled for Cx36 with seven 12-nm gold beads, and for ZO-2 with one 6-nm gold bead (arrow) and three 18-nm gold beads (arrowheads). (D) A long string-type gap junction labeled for Cx36 with many 12-

nm gold beads, and for ZO-2 with eight 6-nm (arrows) and four 18-nm (arrowheads) gold beads. Scale bars=0.1 μm.

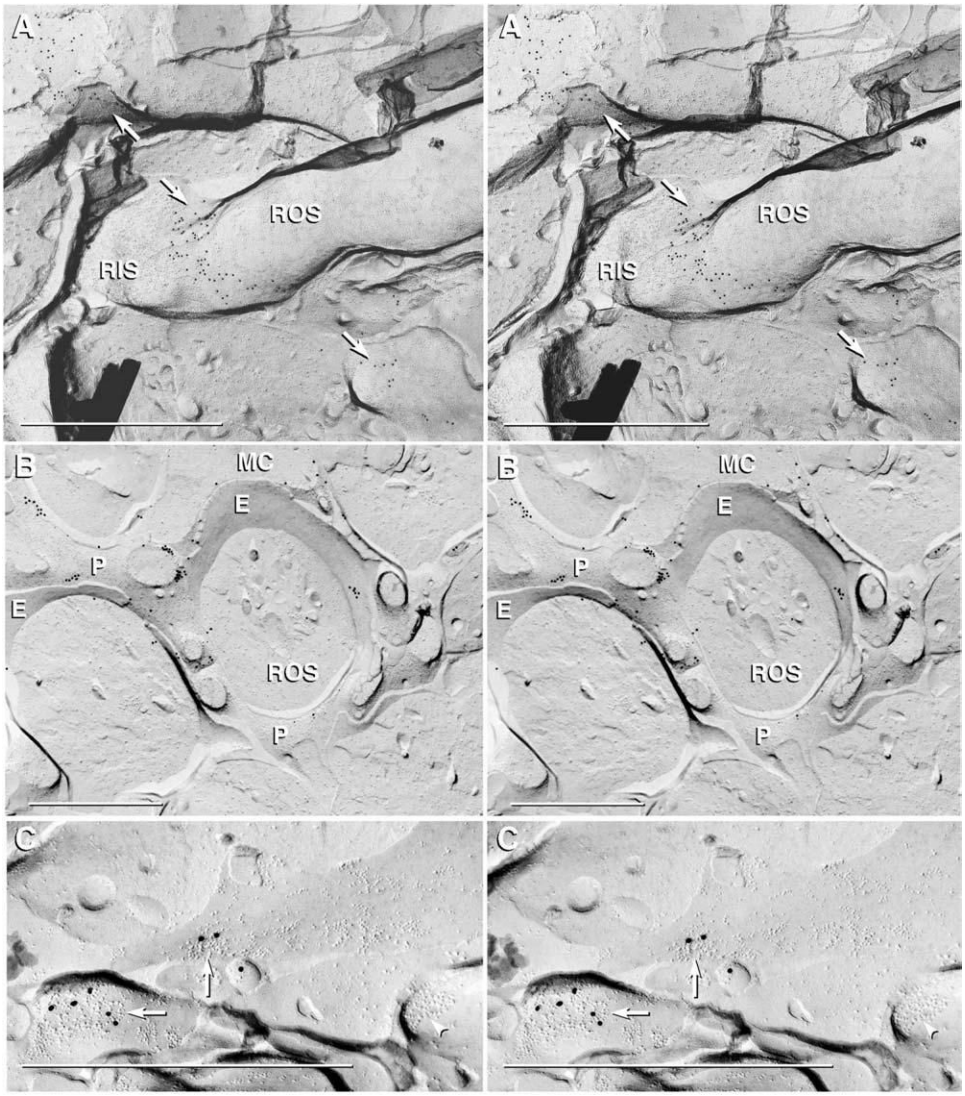

Fig. 7.

FRIL of ZO-1 associated with the OLM, a structure defined as a narrowing between the RIS and ROS. (A) A high density of immunogold beads (arrows) is shown concentrated within the rod cytoplasm in the constricted area of the rod initial segment defines the freeze-fracture correlate of the OLM. (B) Equally abundant gold beads for ZO-1 are seen within the Müller cell (MC) cytoplasm at the level of the MC "collar" that surrounds, adheres to, and constricts the rod initial shaft. Adherens junctions are present, but neither gap junctions nor tight junctions were evident at the OLM. P, MC P-face; E, rod E-face. (C) ZO-1 labeling beneath clusters of P-face IMPs of a PSD (arrows), but not beneath E-face IMPs characteristic of NMDA and AMPA glutamate receptors (arrowhead). Scale bars=1 μm.

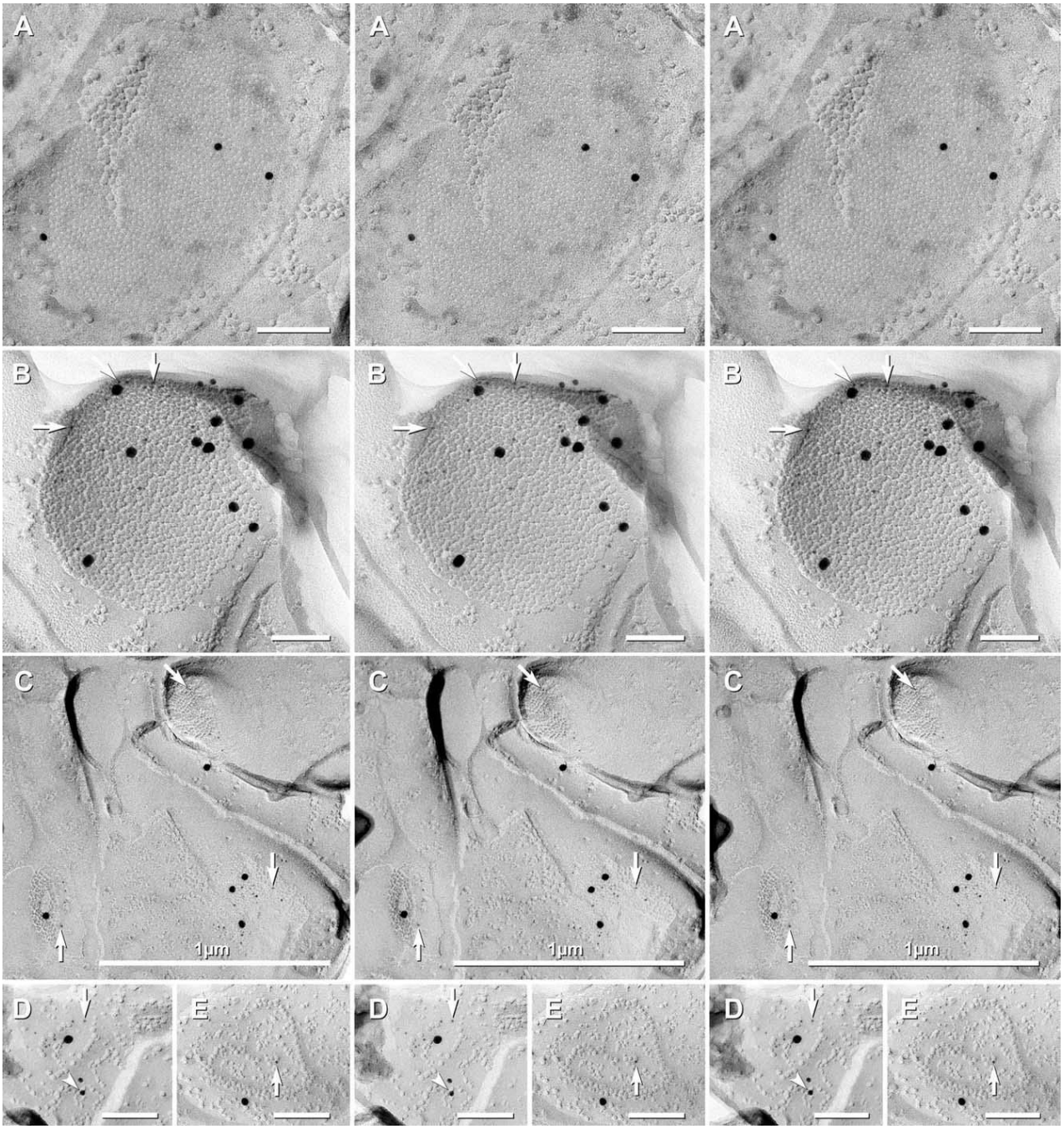

Fig. 8.

FRIL of gap junctions in a replica of rat retina after double-labeling for Cx36 and ZONAB. (A) E-face image of a large crystalline plaque gap junction on neuron in mid IPL, labeled only for Cx36 (three 12-nm gold beads; none for ZONAB). Stereoscopy reveal that a single dark dot (debris) resembling a 6-nm gold bead is on the upper surface of the replica, and is therefore not any type of label. (B) A large plaque-type gap junction in the inner IPL double-labeled for Cx36 (two 12-nm gold beads) and for ZONAB (24 6-nm gold beads, arrows, and 10 18-nm gold beads). (C) Three plaque gap junctions with immunogold labeling for ZONAB (6-nm gold beads, arrows, and 18-nm gold beads) and absence of labeling for Cx36 (12-nm gold beads; none present). (D) Small string gap junction double-labeled for Cx36 (12-nm gold beads,

arrowhead) and for ZONAB (6-nm, arrow, and 18-nm gold beads). (E) Small ribbon gap junction labeled only for ZONAB (one 6-nm, arrow, and one 18-nm gold bead). Scale bars=0.1 μm.

Table 1

Antibodies used for Western blotting and immunohistochemistry

Antibody	Type	Species	Epitope; designation	Dilution	Source
Cx36	Polyclonal	Rabbit	c-Terminus; 36-4600	1 μg/ml	Invitrogen/Zymed
Cx36	Monoclonal	Mouse	Mid-region; 37-4600	3 μg/ml	Invitrogen/Zymed
Cx36	Polyclonal	Rabbit	Mid-region; 51-6300	1 μg/ml	Invitrogen/Zymed
ZONAB	Polyclonal	Rabbit	c-Terminus; 40-2800	2 μg/ml	Invitrogen/Zymed
ZO-1	Polyclonal	Rabbit	aa 463-1109; 61-7300	1 μg/ml	Invitrogen/Zymed
ZO-1	Monoclonal	Mouse	aa 334-634; 33-9100	4 μg/ml	Invitrogen/Zymed
ZO-2	Monoclonal	Mouse	aa 87-208; 611561	3 μg/ml	BD Biosciences
ZO-2	Polyclonal	Rabbit	aa Mid-region; 71-1400	3 μg/ml	Invitrogen/Zymed
Calretinin	Polyclonal	Goat	Whole protein; Ab1550	1:3000	Chemicon

aa, Amino acids.

Table 2

Quantitative analysis of co-localization relationships between Cx36, ZO-1, ZO-2 and ZONAB in the IPL of mouse retina

Proteins examined	Protein (total puncta counted)[a]	Percent co-localization[b]
Cx36 positive for ZO-1	Cx36 (699)	79±7.5
Cx36 positive for ZONAB	Cx36 (1188)	39±2.3
ZONAB positive for ZO-1	ZONAB (884)	44±4.0
ZO-2 positive for Cx36	ZO-2 (591)	93±1.0
ZO-2 positive for ZONAB	ZO-2 (571)	94±0.7
ZO-2 positive for ZO-1	ZO-2 (362)	88±2.2
Cx36 positive for ZO-2	Cx36 (1997)	29±3.5

[a] For each protein indicated, values in parentheses represent the total number of puncta counted in five or six separate single confocal scans of the IPL.

[b] Values represent means±S.E.M. of five or six images examined.